

Antenna Testing Range Team

Final Report

Spring Semester 2023

Senior design Team members:

Adam Hulse: Electrical Engineer

Parker Segelhorst: Computer Engineer

Josh Barber: Computer Engineer

Donovan Wells: Mechanical Engineer

Owen Dietrich: Mechanical Engineer

Department of Electrical and Computer Engineering
Colorado State University
Fort Collins, Colorado 80523

Project Advisor: Dr. Notaros, Branislav

Approved by: Dr. Notaros, Branislav

Date of Approval:

Abstract

Colorado State University houses its own personal antenna test range that is run by students every year to improve their understanding of electromagnetics and radio frequency under the guidance of a world-renowned professor. Electromagnetics and RF are very important to many aspects of daily life from telecommunications to the radios in vehicles. A critical part of these systems are the way they physically communicate between one another, and this is done through antennas and propagation of electromagnetic waves. All antennas emit differently and it is characteristic to the antenna itself. To accurately display these radiation patterns, antennas need to be placed in an electromagnetically isolated environment, shielded from outside RF radiation. This is where the primary importance of an ATR lies.

The current CSU ATR team has embraced the challenging and open ended project by conceiving of various improvements and modifications to make on the ATR, mechanically, electrically and computationally. Some members of the CSU ATR embarked on improving the data storage mechanism for the CSU ATR via redundant storage. Other members of the CSU ATR devoted their time to making custom mechanical antenna mounts in order to increase the accuracy of the ATR measurements, increase the range of antenna types that could be mounted, and to provide a collaborative environment via allowing other teams to measure their equipment within the CSU ATR. Finally, some members devoted their efforts toward developing a transformation process that produces information regarding behavior of the RF radiation patterns measured in the ATR in a much more applicable environment for antennas.

The principal findings of the current CSU ATR are, strictly speaking, tangible improvements on the operation and application of the facility. Given redundant data storage, all ATR data can now be safely recorded and stored for future use. Given mechanical improvements on the antenna mounting mechanism, different antenna types can be used in addition to the increase in measurement accuracy. Given a transformation process that describes the behavior of RF radiation patterns in a more applicable environment for antennas, the ATR can now provide more realistic information for the behavior of various antennas in the real world. While all of these improvements have been a substantial accomplishment for the team, the improvements themselves can be improved by future CSU ATR teams.

Table of Contents

Chapter 1: Introduction.....	1
Chapter 2: Redundant Storage and Server Integration.....	3
2.1 Introduction: Redundant Storage and Server Integration.....	3
2.2 Summary of Previous Work: Redundant Storage and Server Integration.....	3
2.3 Software Design: Redundant Storage and Server Integration.....	3
2.4 Future Work: Redundant Storage and Server Integration.....	3
Chapter 3: Motor Controller Case and Upgrades.....	4
3.1 Introduction: Motor Controller Case.....	4
3.2 Summary of Previous Work: Motor Controller Case.....	4
3.3 Hardware Design: Motor Controller Chassis.....	5
3.4 Future Work: Motor Controller Case.....	7
3.5 Motor controller upgrades - Motor controller boards.....	8
3.6 Motor controller upgrades - Relay for remote start.....	9
Chapter 4: Live Camera Feed of ATR.....	11
4.1 Introduction: Live Camera Feed of ATR.....	11
4.2 Previous Work: Live Camera Feed of ATR.....	11
4.3 System Configuration.....	11
4.4 Future Work: Live Camera Feed of ATR.....	11
Chapter 5: Universal Antenna Mount.....	12
5.1 Introduction: Universal Antenna Mount.....	12
5.2 Summary of Previous Work: Universal Antenna Mount.....	12
5.3 Hardware Design: Universal Antenna Mount.....	13
5.4 Hardware Manufacturing: Universal Antenna Mount.....	17
5.5 Results: Universal Antenna Mount.....	17
Chapter 6: Near-field to Far-field Transform.....	19
6.1 Introduction: Near-field to Far-field Transform.....	19
6.2 Summary of Previous Work: Near-field to Far-field Transform.....	19
6.3 Objectives: Near-field to Far-field.....	20
6.4 Transform.....	20
6.5 Results.....	22
6.6 Software.....	25
6.7 Software Capabilities.....	26

6.8 Notable Observations.....	26
Chapter 7: 5-Element Patch Antenna Array.....	29
7.1 Goals of Design.....	29
7.2 Background Information.....	29
7.3 Calculating lengths of patch and position of rear-feed line.....	31
7.4 Simulation.....	33
7.4.1 Simulation of patch antenna.....	33
7.4.2 Simulation of 5-element patch antenna array.....	34
7.5 Generating Gerber Files for PCB.....	37
7.6 Antenna Test Range Measurements.....	37
7.7 Wrapping It All Up.....	38
Chapter 8: Standards.....	39
Chapter 9: Conclusion.....	40
Chapter 9: Future Work.....	41
9.1 Future Work: Motor Controller Case and Upgrades.....	41
9.2 Future Work: Universal Antenna Mount.....	41
9.3 Future Work: Near-field to Far-field Transform.....	41
Appendix A- Abbreviations.....	43
Appendix B- Budget.....	44
Appendix C- Project Plan Evolution.....	45
Appendix D: Universal Antenna Mount Drawings.....	49
Appendix E: NF->FF Software Operation & Troubleshooting.....	54
How to Use NF->FF.....	54
NF->FF Troubleshooting.....	55
ACKNOWLEDGEMENTS.....	56

Chapter 1: Introduction

Antenna Test Ranges are essential radio frequency testing environments, often located in prominent university and industrial facilities. ATRs are used to measure radiation distribution patterns and performance of antennas in an electromagnetically isolated environment. Their applications are broad as antenna performance plays a critical role in modern society.

Given the broad applications of ATRs, their effect on the field of electromagnetics cannot be understated. While ideal radio frequency radiation distributions can be theoretically computed, their actual isolated behavior can only be measured in an ATR given that our planet is now filled with radio waves propagated in all directions.

A particularly intriguing application of an ATR has been NASAs Antenna Test Facility. Used for the currently ongoing Artemis program, the Orion space capsule was placed in an anechoic chamber, similar to the one used in the CSU ATR. The purpose of this experiment was to measure the behavior of different antenna configurations for the Orion space capsule.

The CSU ATR itself has been the subject of many different overarching goals: from education, to applicable antenna measurements, to collaboration amongst multiple senior design teams. Each ATR senior design team has the opportunity to embark on their choice of project goals.

Designed and constructed in 2008, the CSU ATR has since been developed and improved on by several generations of senior design teams, each with their own respective modifications and adjustments. The CSU ATR is a lenient senior design project that allows team members to determine, mostly amongst themselves, what sort of improvements or modifications that would like to make. There are often several partially completed, or even just prospective projects, passed down from generation to generation of CSU ATR teams as recommendations, but nothing particularly is required.

Because of the unrestricted nature of the project, each member of the current, large, interdisciplinary, five person team embarked on their own projects that contributed to the overall improvement of the ATR. Listed below is how the subsequent report separates each sub-project amongst the different members of the ATR.

Chapter 2: Redundant Storage and Server Integration

- This project was headed by Josh Barber, a computer engineering student. An overview for the purpose of this project was to include a redundant ATR scan data storage mechanism that prevents loss of data due to HDD failure. It also allows for ATR scan long term storage for subsequent teams to use.

Chapter 3: Motor Controller Case and upgrades

- This project was headed by Owen Dietrich, a mechanical engineering student. An overview for the purpose of this project was to provide a case surrounding the ATR motor controller. The idea was to mitigate exposed wiring to protect both the ATR team from shock and to protect the motor controller from the ATR team potentially damaging

connections on the motor controller. While designing this case other motor controller problems arose that needed to be fixed.

Chapter 4: Live Camera Feed of ATR

- This project was headed by Donovan Wells, a mechanical engineering student. An overview for the purpose of this project was to provide a live CCTV camera feed of the ATR interior chamber. The advantage of integrating this quality of life fix was to provide users of the ATR with the ability to see the positional adjustments made in the ATR interior without needing to go inside the ATR interior every time a positional adjustment was made.

Chapter 5: Antenna Aperture Mount

- This project was also headed by Donovan Wells and Owen Dietrich, both mechanical engineers. After professional feedback of the ATR interior, one of the primary concerns regarding measurement functionality was that one of the antenna faces was not aligned with the center of rotation of that antenna's φ -axis. By reconstructing the mount for that antenna, the antenna face could be made to align with its center of rotation, thus providing more accurate RF radiation distribution patterns. Additionally, this new mounting mechanism could be made to fit several types of antenna, not just exclusively the horn antenna which all previous ATR teams had been subjected to use. By making the new mounting mechanism customizable to different antenna types, the ATR team could collaborate with the MRI senior design team in letting them scan their MRI coil within the ATR.

Chapter 6: Near-field to Far-field Transformation

- This project was a collaboration between Adam Hulse and Parker Segelhorst, both electrical and computer engineering students respectively. This project was intended to provide future ATR teams with an easy-to-use software for EM field plotting and manipulation. The purpose of this contribution to the ATR is that it would allow for more applicable measurements of RF radiation distribution patterns as the transformation algorithm itself provides information regarding RF radiation distribution patterns in the more commonly utilized far-field.

Chapter 7: 5-Element Patch Antenna Array

- This project was headed by Adam Hulse, an electrical engineering student. An objective of the ATR this semester was to use the ATR with an antenna beyond the horn antenna that has been used for the previous teams. Therefore a new antenna was to be developed to employ theories learned from CSU and apply it to a real patch antenna array.

Chapter 2: Redundant Storage and Server Integration

2.1 Introduction: Redundant Storage and Server Integration

The initial storage method for saving scans was to put them on the laptop that was running the scan. This made sharing scans between generations of the ATR impossible and no reliable backup for the saved scans. In order to create a safe and redundant storage space, extra space was added into the PC in the ATR. There was also no way to compare the data from multiple scans together so a server instance was made on the ATR PC.

2.2 Summary of Previous Work: Redundant Storage and Server Integration

There was previously no form of redundant storage in the ATR. The only hardware that was in the lab was the PC itself. Previous teams had always used personal laptops to run scans and store scan data while the ATR PC was sitting as an unused asset.

2.3 Software Design: Redundant Storage and Server Integration

Starting with upgrading the ATR PC our team installed 4TB of HDD storage and downloaded SQLServerExpress. This extra space allowed us to store many scans which can be accessed by future ATR teams. Using the SQLServerExpress instance, a database was created which could access all the data stored on the HDD and can perform data analysis with a series of SQL queries.

To establish redundancy our data storage utilized Google Drive to make a cloud based copy of all our data. This was easily done by creating an ATR google account, then downloading the Google Drive application onto the PC. This app allows you to connect your folders to Google Drive such that you can access them remotely and have a backup in case the HDD fails.

2.4 Future Work: Redundant Storage and Server Integration

This current storage method works well but could use upgrades. The Google Drive method for storing data redundancy only can store up to 15GB of data. This means that if more than 15GB of stored data is in the ATR PC the oldest files would be pushed off the Google Drive. Instead a different free server hosting tool could be used (Such as a window OneDrive) or another 4TB of storage could be added to the ATR PC such that a RAID like redundancy could be set up on the PC itself.

With respect to the SQL server the current use is very limited since the .txt files generated from scans have little use being compared since each data point is a small slice of the entire scan. If a query could allow for multiple point analysis or possibly comparing the data after processing, it could lead to a better utilization of the server and possibly give us a good way to compare ideal values to measured values in a short amount of time.

Chapter 3: Motor Controller Case and Upgrades

3.1 Introduction: Motor Controller Case

The antenna motor controller systems used to adjust the positioning of the receiver and transmitter are controlled by two high speed optocoupler stepper motor driver 4 axis CNC controller boards and an electronics screw terminal block all powered by a 24 V power source plugged into an AC outlet. This controller system is crucial to the antenna testing range in that it operates all of the mechanical components located in the anechoic chamber.

Increasing the accuracy and reliability of the antenna testing range is a primary goal for further development of the project for all future endeavors thus the primary components must be working according with high precision and accuracy. To increase the accuracy, precision, durability, and reliability of the system, the control boards need to be protected from environmental sources such as increased ambient temperatures of the air and human interference. The antenna motor controller case needs to ensure the protection of the electronic equipment from human and environmental sources.

3.2 Summary of Previous Work: Motor Controller Case

Antenna Test Range teams in the past years attempted to address the issue of the lack of protection from potential sources impacting the controller case. Initially, the controller case was enclosed in a plexiglass container, allowing easy viewing access and utilizing the working space in a more optimal manner. Previous teams failed to address the ventilation system of the structure, thus the ambient temperature inside the system frequently affected the electronic components causing overheating and catastrophic failures. The catastrophic failures proceeded to affect the durability of the case itself by burning the container walls due to the low heat resistivity variable of the material. This design succeeded in enclosing the electronic components in a small structure; however, the motor controller case did not address the ventilation system, causing an increased risk of failure.

The ATR team of 2021 reengaged the motor controller project in an attempt to quickly address the issues of the previous design. A quick solution was required since the construction of the motor controller case required the antenna testing range to be inoperable which is not ideal. The solution was to mount the electronic components using various fasteners to a plexiglass board. Each of the electronic components are elevated off the surface of the plastic to increase the amount of air under the boards to increase potential air flow under the system to reduce potential heat sources from the board failing.

Additionally, heat sinks were bought and mounted to the top of the boards to increase the flow of heat away from the potential heat sources located on the boards. To circulate the air around the heat sinks mounted on the CNC controller boards, a small 5V ball bearing fan was placed on each heat sink. The fans were placed in such a manner that the air flow was not optimized to remove the heated air surrounding this component in that the direction of the fins were perpendicular to the direction of air flow rather than parallel. In addition to the unoptimized heat sinks, there was no protection around the electronic components thus potential impact from

human error was still inevitable. The system was powered using an outlet which decreased quality of life. The ATR tema of 2022 hoped to address these issues and further develop the project.

3.3 Hardware Design: Motor Controller Chassis

Embarking on the motor controller chassis project, there were several factors that needed to be accounted for including the ventilation system, material used to manufacture the case, general overall aesthetic of the design, ease of access of the electronic components housed in the structure, and optimizing the working space while still attempting to minimize cost by utilizing available parts in the lab. The chassis utilized a Dell OptiPlex GX280 as the main frame for the motor controller case. An analysis of the fluid dynamics characteristics of the structure originally was determined using the software program Ansys. A basic cross section was created and a working fluid was put through the system while incorporating the standard fan located in the center of the structure which can be seen in the figure below.

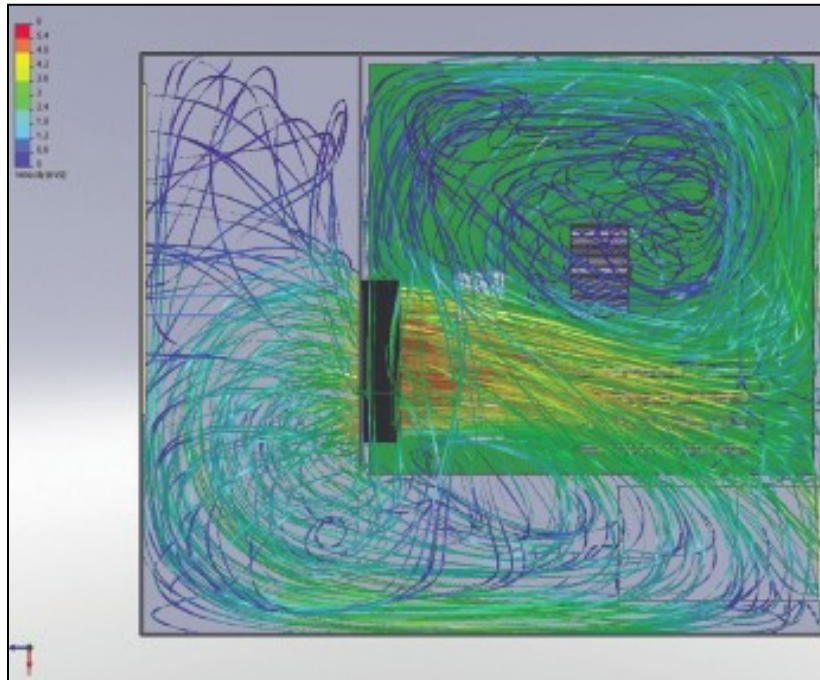


(Figure 3.1: CFD Analysis of Dell OptiPlex GX280 Computer Desktop Case)

When the working fluid is circulating by the work being done on the surrounding air by the computer fan, the flow of the air appears to be chaotic. The turbulent flow in the upper right hand corner can be observed which causes the formation of vortices. When attempting to cool the electronic components to maintain a constant ambient air temperature, vortices limit this factor because the air stream has nowhere to go thus the air begins to rotate in a circular pattern. To reduce the formation of vortices in the system, the minimization of the compartmentalized structure inside the case was implemented in addition to improving the ventilation system of the side panels. The front and rear panels had a noticeably lower temperature than that of other parts of the structure. This observation allowed the front and rear panels to be manufactured using the

additive manufacturing process using materials with a low heat resistivity. Using PLA, the front and rear panels were 3D-printed in multiple parts to account for the limited printing bed size. After minimizing the compartmentalized structure inside the case, supports and rail systems were created using subtractive manufacturing processes such as using the CNC to create rails and abrasive cutting machines to form shelves. The first design can be seen in the figure below. This model was designed using the software program Solidworks which is provided to the mechanical engineering students at Colorado State University.

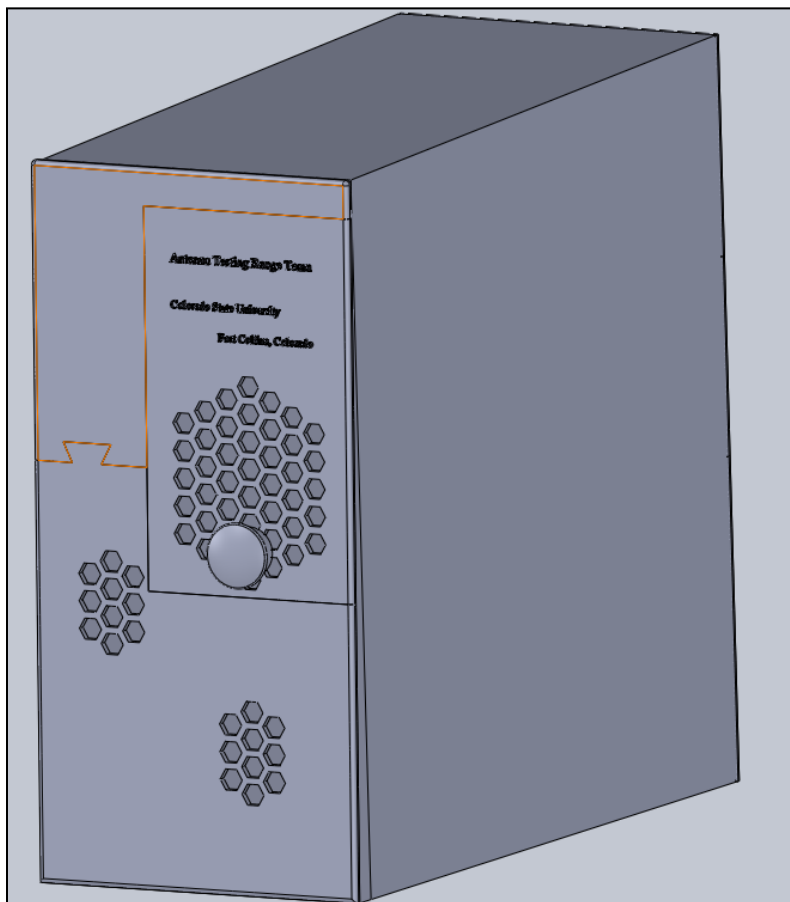


(Figure 3.2: Original Motor Controller Case Design)

The first motor controller case design incorporated additional ventilation ports on the front and rear panels to increase the amount of laminar flow throughout the system. A drawer was designed to position the motor controller boards vertically to appropriately fit the electronic components on the shelf. Several ports were incorporated on the rear of the motor controller case to allow access for the remote on and off switch, motor cable connection points, and the power source cables.

This design utilized 3 dual ball bearing computer fans such that two of the fans directed air into the system and a single fan was used to move air out of the system. A CFD simulation was run on the new current model to determine the mass flow rate of the system, as well as the formation of vortices. The mass flow rate of the system, ratio of the air coming into the structure and out of

the structure, and the working fluid behavior was determined. The ratio of the air coming into the system was determined to be 1.4 which demonstrates that more air is coming into the system than that is leaving which is expected due to the ratio of fans used to push air in and out of the system. The working fluid was able to move across the electronic components with minimal turbulent flow.

After conducting a thermocouple analysis, the ambient temperature remained relatively constant of the duration of a standard operation period of 30 minutes while only having a temperature deflection of 6 degrees Fahrenheit over the entire duration.

While the new device succeeded in obtaining optimal fluid characteristics simulated using a CFD analysis and maintaining a relatively constant temperature inside the device, more modifications were necessary after the short implementation of the device. The orientation of the motor controller boards was originally designed so that the heat sink located on the top of the motor controller board is perpendicular to the current of the air caused by the computer fans on the upper level. The original thought process behind the orientation of the boards was primarily due to wire management and creating turbulent flow around the heat sinks to increase the amount of time that the cool air is in contact with the boards. Then the lower fan on the bottom level of the device would move the air outside the case.

To increase the system's overall efficiency, it was determined that the position of the heat sinks were altered so that they were parallel to the current of air, allowing air to flow more easily around the boards. Additionally, access ports on top of the case with the integrated locking mechanisms were added to increase the accessibility of the pin boards.

Modifications to the drawer system need to be implemented to increase the quality of life for the operator and ease of use of the system. Furthermore, the device not only had to function properly, the device had to easily be used as a demonstration feature for outreach programs coming to the antenna testing range at Colorado State University to further understand electromagnetics and antenna systems.

3.4 Future Work: Motor Controller Case

Due to the change in customer requirements of the design, the future of the motor controller case chassis came into question. The current device failed to be a demonstration feature of the ATR for outreach programs due to the original goal to maximize the working space by minimizing the surface area that the device occupies. Additionally, the material used to make the case is opaque which prevents the observer from viewing the device components with complete disassembly of the device.

The fasteners used to assemble the device also posed a potential issue with safety due to the sharp edges protruding from inside the drive. These protrusions cause safety hazards when attempting to maintain or work on the device. Due to the time frame of future projects in the ATR and the requirement to use the motor controller case as a demonstration piece, the current motor controller case project is terminated and will not be continued to the following semester.

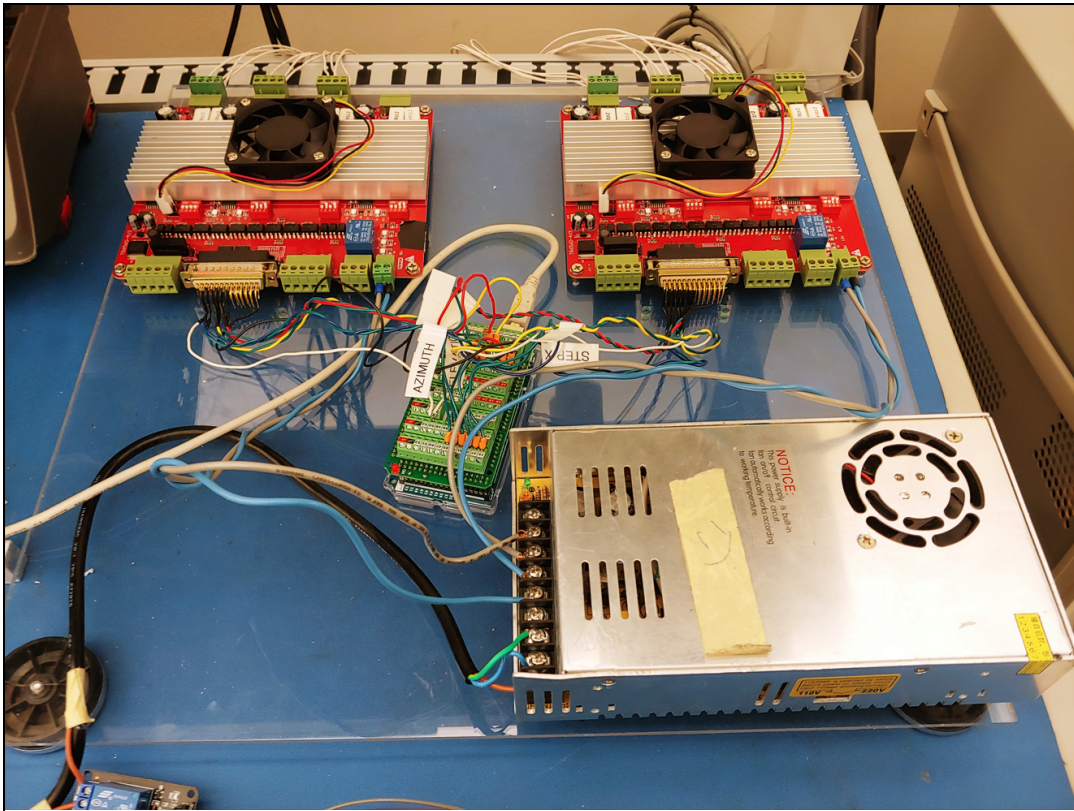
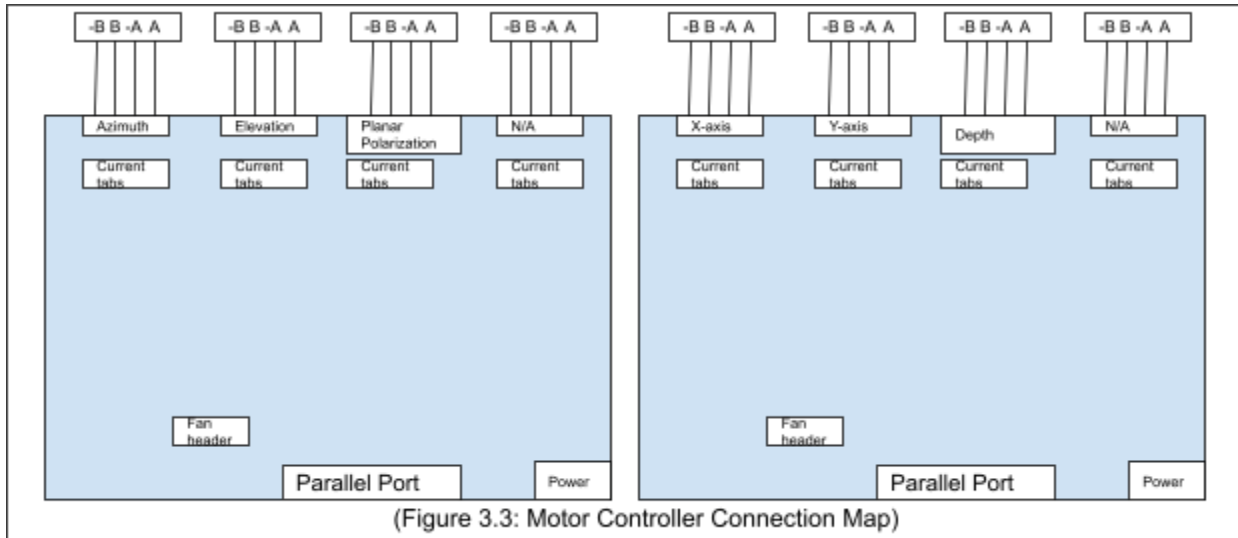


(Figure 3.3: Current Motor Controller Layout)

The original format of the motor controller boards and electrical components is currently being used. This solution, as seen in the figure above, is extremely easy to reference particular components for demonstration purposes and for outreach programs. Additionally, the ease of maintenance is very ideal in that everything is accessible. There is currently still a potential for environmental impacts and human collision; however, excess caution will be used around the system to ensure the device is not impacted. Since the continuation of the motor controller case ended during the fall semester of 2022, efforts were placed on future projects such as arraying antenna frames and improving functionality of the ATR in the spring semester of 2023.

3.5 Motor controller upgrades - Motor controller boards

At the beginning of the semester the ATR team performed a functional evaluation of the range to be able to determine the current functionality left from the previous team. It was discovered that the polarization motor within the range wasn't enabled due to a broken port on the motor controller. This was a problem since the lab was acting as a 5 axis scanning mechanism when the code and design was for 6 axis. To fix this new motor controllers were ordered and installed with the same connections as the previous set up. The new controllers were the TB6560 4 axis Nema 23 board with a TB6560AHQ chip. The board was ordered from amazon from a 3rd party manufacturer that had higher user rating when using Nema 23 motors which helped reduce the cost of fixing the problem. The first step in installing the boards was creating a wiring diagram such that no connections were misplaced when the installation occurred and the code would not need alteration.



After the installation of the new motor controller boards there was a problem that was found out by the MRI while attempting to use the range. The motors were emitting a whine when trying to perform a scan. Attempts to switch back to the old motor controller board didn't seem to fix these issues. Finally we once again swapped the old boards to the new and the lab started to work. The issue could have been due to the current tabs not being set to allow the correct amount of current to the stepper motors and when the lower current was sent to the motors and they attempted to start the current wasn't enough to get past the starting threshold. After waiting long enough for the motor to reset itself and swapping the boards to the new controllers again, with the correct current settings, we were able to get the lab running correctly with the polarization motor working.

3.6 Motor controller upgrades - Relay for remote start

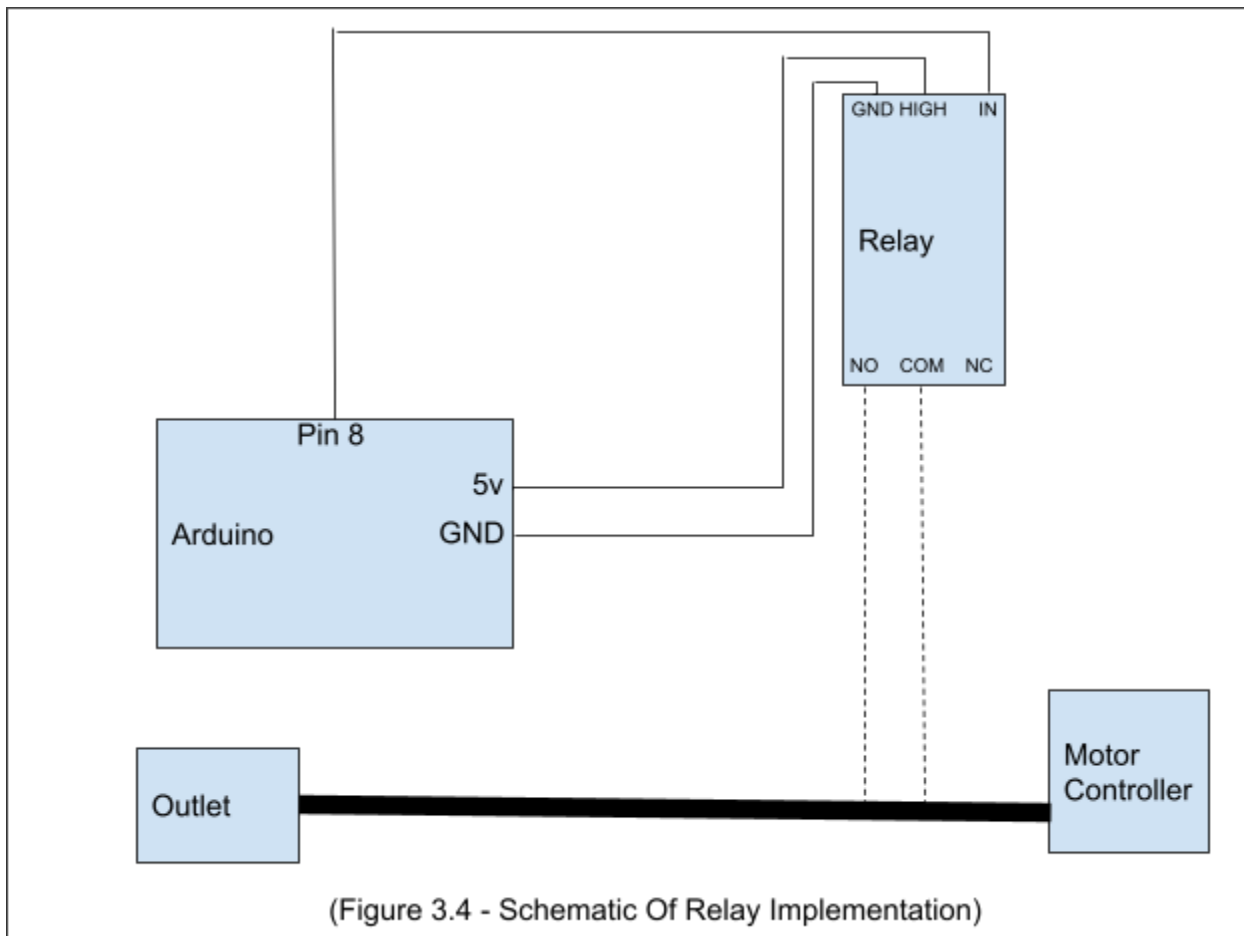
One idea we had for upgrading the QoL for the lab was enabling the lab to be run remotely, meaning that if someone wanted to perform a scan using the ATR they wouldn't need to be inside the lab but instead could operate the lab from home. This required several updates to the lab, one of which was the ability to turn on/off the motor controllers using a relay connected to the lab PC.

The first step was testing the relay provided by one of the team members, this was done using a breadboard and LED along with an arduino. The set up for the relay needed to be a normally open connection which has the contacts disconnected until the correct pin is power which enables a electromagnet to pull down another contact completing the circuit and allowing current flow. Putting this on the breadboard with the arduino the team wired the normally open connections to each side of the LED and used an addressable pin on the arduino connected to the input of the relay. The relay also took in the 5v and GND pin as references to determine the electromagnet threshold. Coding the Arduino to work properly was an easy task since there are many guides online on how to do so by selecting a pin on the Arduino to power the relay and

enabling a high signal to the pin. Testing of the relay and Arduino showed that the relay was functioning properly with the code and we went on to connect the relay to the motor controller.

Since the motor controller uses the wall outlet safety was a major concern while working on the high voltage wire. To avoid any injuries all power connections to the motor controller were disconnected while working on the wire.

To allow the relay to act as a current blocker the wire was cut open and the hot wire inside was also cut. The hot wire was stripped and the ends were put into the open connections of the relay. Then the wire was plugged back into the wall outlet and the ATR PC was connected to the Arduino. Testing of the relay while connected to the motor controller showed that the functionality was as intended where the ATR pc could upload a on/off code to the arduino which would then turn on the motor controller.



Chapter 4: Live Camera Feed of ATR

4.1 Introduction: Live Camera Feed of ATR

The ATR is a fully insulated room, designed to act as a Faraday cage, fully isolating any internal EM emissions for the purpose of measuring them in some way. As such, the room has no windows, and anything inside cannot be observed without physically entering the room. This has been an issue in the past, as the positions of any components must be verified both before and during a scan. These positions cannot be verified during a scan, as opening the door changes the noise level in the room and results in leakage, causing any scan data to be skewed. If a mechanical component were to malfunction or break, the operator would not know until after the scan has completed, and the room can be entered. The lack of visibility also poses a safety risk, as there is no way to open the chamber door from the inside, and no sound can enter or leave the chamber. This means that there is no way to know if a person is stuck inside the chamber. It was determined that a live camera feed within the room was a good solution to these problems.

4.2 Previous Work: Live Camera Feed of ATR

A previous ATR team acquired usb webcams to place in the chamber. They also installed these cameras in the room by nestling them inside of the ceiling insulation at two locations. The cables for these cameras were run under the insulation, and to the outside of the chamber alongside the motor wires. The previous team did not configure these cameras to display the feed, as the cameras need to be connected to a PC in order to display their feed, and used outdated control software.

4.3 System Configuration

The cameras already installed in the chamber were used to display the live feed. The cameras needed to be connected to a PC in order to display the feed, but this feed could not be displayed at all times without its own dedicated device. Using a Raspberry Pi, it became possible to receive the feed from both cameras in the chamber and display them on a monitor on the outside of the chamber. Research was done into several softwares that could display this feed, and the final decision was between VCL and Motion. It was decided to use Motion, as the feed could also be live streamed from the Raspberry Pi and viewed remotely, as long as the viewer is connected to CSU's network.

4.4 Future Work: Live Camera Feed of ATR

The sub-project to incorporate the live camera feed of the ATR is considered complete, and has been useful in performing scans within the chamber. There is some potential work to be done, primarily replacing the cameras used in the chamber. The current cameras have a low resolution and low framerate, causing some detail in the chamber to be missed, and small movements to be difficult to track. If the cameras are to be replaced in the future, the documentation for the system configuration can still be followed, as long as the cameras are compatible with the Raspberry Pi. The software used can also be changed to one that allows the operator to remotely move the cameras, and zoom into specific locations.

Chapter 5: Universal Antenna Mount

5.1 Introduction: Universal Antenna Mount

Early in the fall semester, a Ball Aerospace engineer who serves as the manager for one of Ball's antenna testing facilities came to give advice for how the ATR may be improved. From this meeting, it was determined that the mount that held the transmitting antenna was incorrectly designed, as the face of the antenna was not at the center of rotation. This negatively affects all scan data, as both the position and orientation of the antenna face was changing during scans. The ATR also needed the ability to mount different types of antennas other than horn antennas, especially to test the *Patch Antenna Array*. The MRI team also requested a way to measure the field inside their coil, and as such needed a mount that could do so. The advice from Ball, and the antenna mount were combined into one project, and incorporated together.

5.2 Summary of Previous Work: Universal Antenna Mount

The previous antenna mount (Figure 5.1) was made primarily of aluminum and wood corner molding. It had an aluminum base which connected to a primary support made of PVC and wood, which also had the motor wires running through it. It also used a large number of metallic components, such as bolts and mounting plates. The effect of these metallic components is undetermined, but their presence has some influence on scan results, as their own magnetic fields can influence any EM emissions that are to be measured. The previous antenna mount also had some wobble when rotating about the base, as it only had one primary support away from the center of rotation.

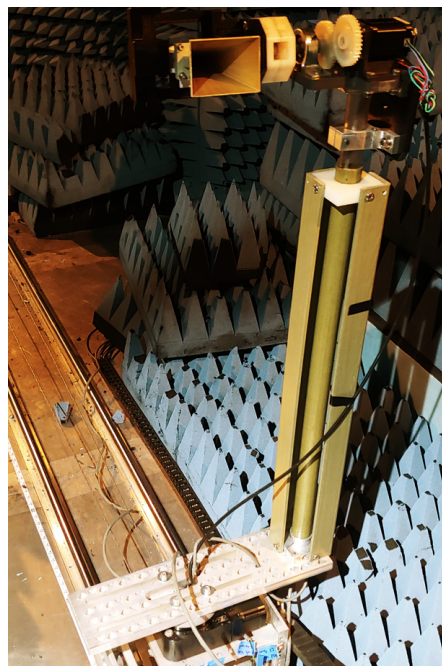


(Figure 5.1: Previous Antenna Mount)

5.3 Hardware Design: Universal Antenna Mount

The new antenna mount was designed to incorporate the advice from Ball, and the MRI team's mount, as well as use as much existing equipment as possible. As such, the design consists of three parts, the frame, the MRI specific mount, and the antenna mount. The Frame was designed to bolt onto the motor at the base, in the same way that the previous mount was connected. It was designed to have greater stability by using two supports on either side of the antenna, which also allows it to bear the weight of the MRI coil. Through research, it was determined that the most cost effective material for the base was wood, so the base and upper platforms were designed to be made from 1 inch thick pine board, and the supports to be made from 30 inch lengths of 2x4s. Wood was chosen because of its completely non-magnetic nature, which helps to keep the noise level down and reduce reflectivity in the ATR.

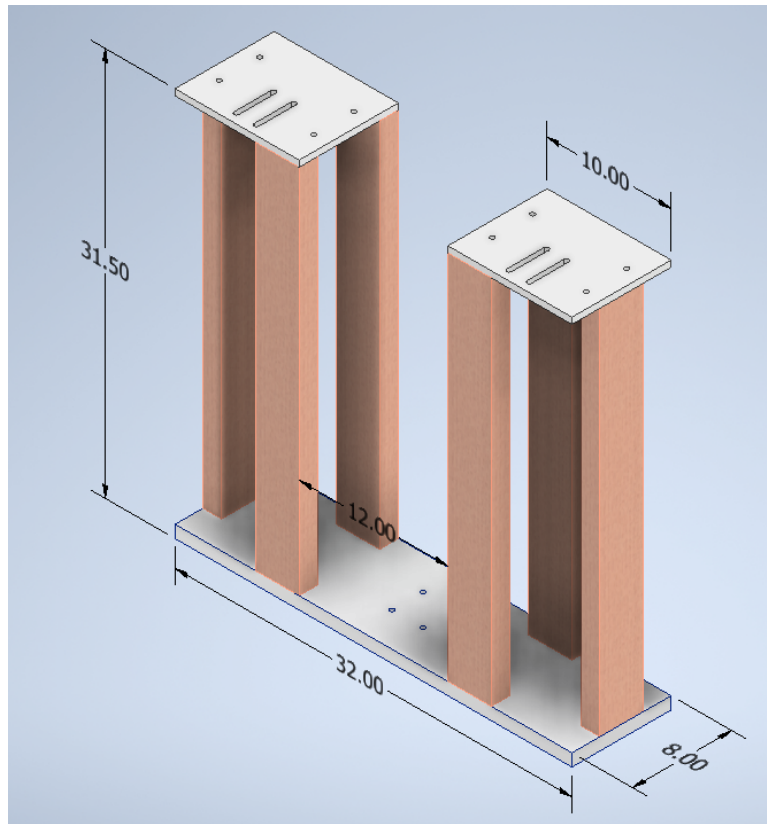


(Figure 5.2: New Frame CAD Model (dimensions in inches))

The MRI coil mount was designed as a simple box shape made of wood that the coil could rest on, which would then be placed on the frame. A simple stress analysis was performed, and verified that the frame could withstand more than 100 lbs of weight before failure, which was significantly higher than the weight of the MRI coil.

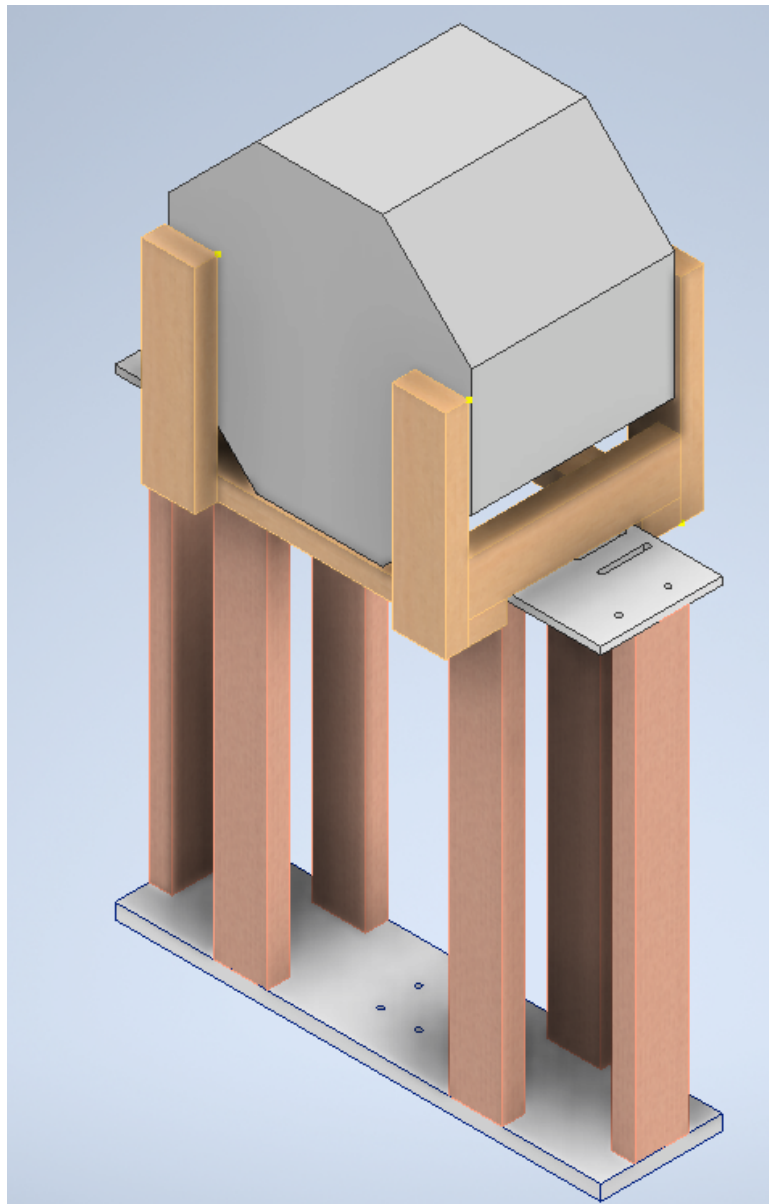


(Figure 5.3: Frame CAD Model With MRI Mount)

To incorporate the center of rotation fix, the antenna mount was designed to support the antenna from the back, and keep the face of the antenna in line with a split shaft which defines the center of rotation. All components of the antenna mount were designed in Autodesk Inventor. The mount was designed to be fully 3D printed (excluding the shaft), due to the low cost and complexity of the parts, and to be able to mount antennas of varying sizes. Detailed drawings of all components are provided in Appendix D.

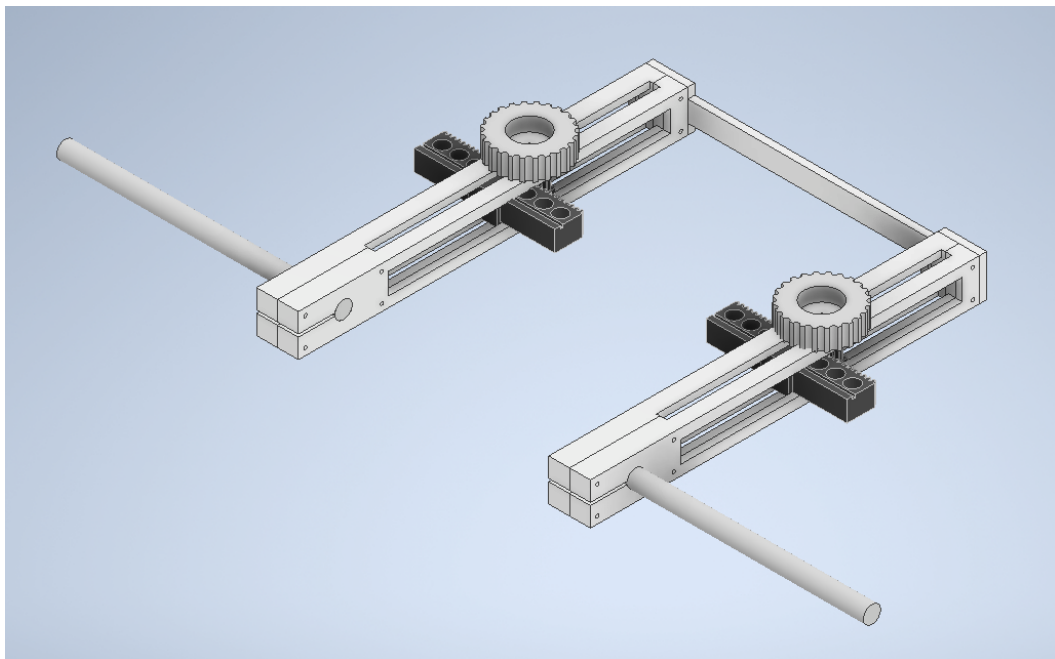


(Figure 5.4: Antenna Mount CAD Assembly)

The antenna mount is made up of two sub-assemblies. The arm assembly connects directly to the motor platforms through the bearing housing attached to the split shaft. The shafts on each side attach to the slotted arms of the mount, which are connected by the shaft connector at the rear of the assembly. Both of the arms are designed to be printed in four pieces, due to dimensional constraints of the 3d printer, and can be glued or screwed together. The slots in the arms allow the mounting point of any antenna in question to be from 1.63 in. to 9.74 in. away from the center of rotation and up to 9 in. wide. Any antenna mounted in this system must fit within this constraint, and specialized mounts can be created to mount an antenna as needed.

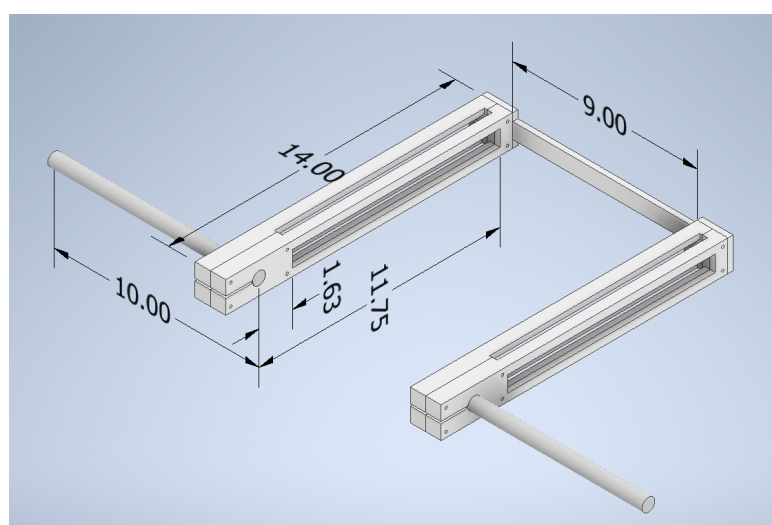


(Figure 5.5: CAD Arm Assembly)

The collar assembly is designed to fit within the slotted arms, and must be installed before the arm assembly is assembled. The collar assembly consists of the collar, which has a key that keeps the rack aligned and in place as it slides through, and contains a pinion gear that interfaces with the rack. A knob with a keyed shaft passes through the top of the slotted arm and through the collar and pinion gear, securing the pinion and transferring force, allowing the rack to be both secured and adjusted as needed. The knob is sized for a square head bolt to pass through it, which can be tightened with a wing nut on the top of the knob, which secures both the rack's position and the collar assembly's position along the slotted arm. The rack has evenly spaced holes through the top and bottom surfaces, which is where specialized antenna mounts can be attached.

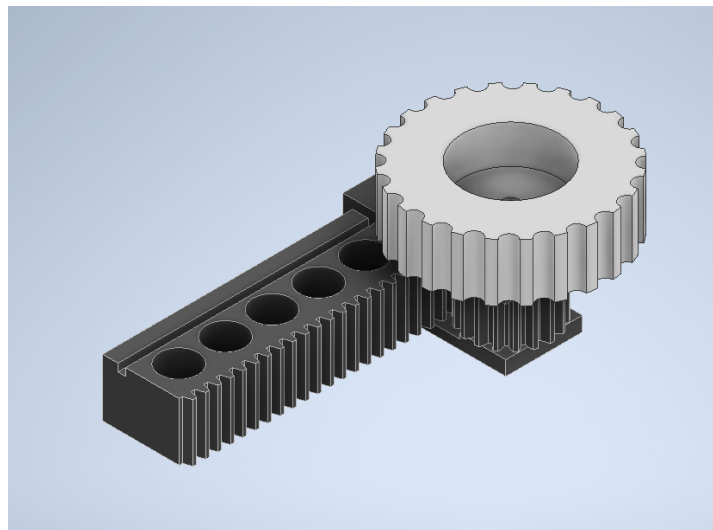


(Figure 5.6: CAD Collar Assembly)

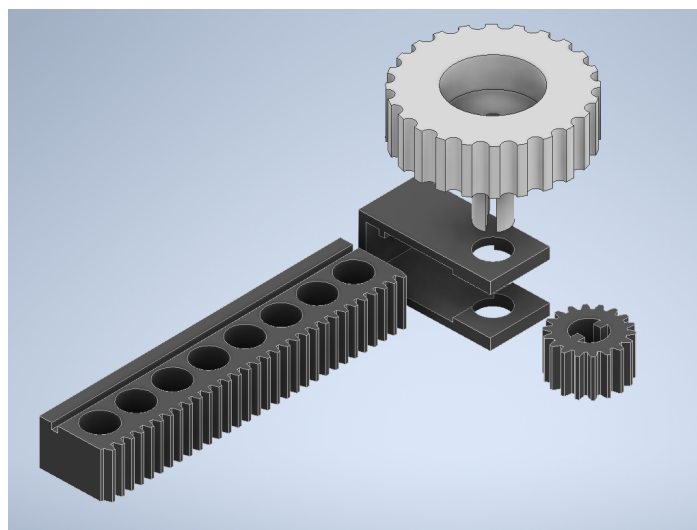


(Figure 5.7: CAD Exploded Collar Assembly)

After initially designing the antenna mount, it was clear that it would be too heavy for the existing motor, as it would weigh close to 12 lbs. As such, a weight optimization process was performed, mainly changing the infill of the 3D print and the thickness of the parts. After optimization, the weight of the mount was lowered to about 3 lbs, assuming a 30% infill. This weight is low enough for the motors to bear, as long as a gear ratio of 1:3 is used. This ratio also includes a factor of safety of 2, meaning that it can provide twice as much torque as is needed to hold the mount stationary at the motor's rated holding torque.

5.4 Hardware Manufacturing: Universal Antenna Mount

The primary method used to manufacture the antenna aperture mount was additive manufacturing. Additive manufacturing was chosen to construct the device due to the minimal cost associated with purchasing the materials, relatively high precision (0.1mm on the z-axis, 0.3mm on the x and y axis), availability of 3D printers for mechanical engineering students, material would not be subjected to high stress loads from the antenna, and the antenna mount would not be exposed to UV light or any other external environmental factors being that the mount will remain in the anechoic chamber at Colorado State University. Furthermore, if future teams decide to replace the antenna mount for a lighter material, PLA is a biodegradable material.

The chosen material to construct the antenna mount is Polylactic acid based plastic (PLA). PLA has a specific density of 1240 kg/m^3 , a yield strength of 53 MPa, and an elastic modulus of 3.5 GPa. For the current antenna aperture design, the antenna is projected to only exhibit a quarter of the yield strength thus falling within the elastic region of the stress strain curve. This will allow teams to increase the antenna size a significant amount without observing any plastic deformation on the device.

Conductive material such as metals and some composites have a negative effect on the electromagnetic fields measured by the Vector Network Analyzer (VNA). The ability to reflect light or radiation is a negative characteristic of materials when considering the application of the ATR team's antenna mount. Metals generally have a high reflectivity rate as compared to PLA which has a reflectance rate of about 60% while plastic tends to have a reflectance of about 4% which is ideal for measuring antenna radiation patterns.

5.5 Results: Universal Antenna Mount

After taking into consideration Ball Aerospace's recommendations and successfully implementing the antenna aperture mount, the results gathered from the vector network analyzer significantly increased in persians and accuracy. Previously, the antenna face was not centered over the axis of rotation thus when conducting a polarization scan of an antenna thus the antenna face was being swept over a larger area rather than pivoting around a point. This error was causing the electromagnetic scans to appear wider which can be seen in figure 5.8 below.

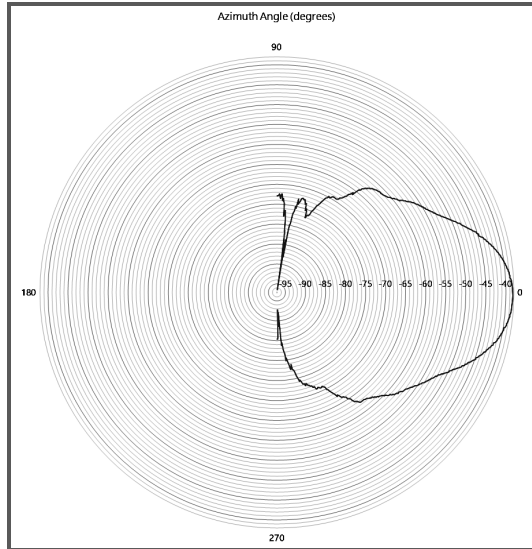


(Figure 5.8: Azimuth scan of horn antenna before modifications)

The radiation pattern appears to have a more round structure and has some variability near the center of the graph. Some variability can be expected but should be symmetric about the horizontal plane. After constructing the new antenna mount, placing the face of the antenna over the axis of rotation, the radiation pattern core closely resembled simulated radiation patterns.

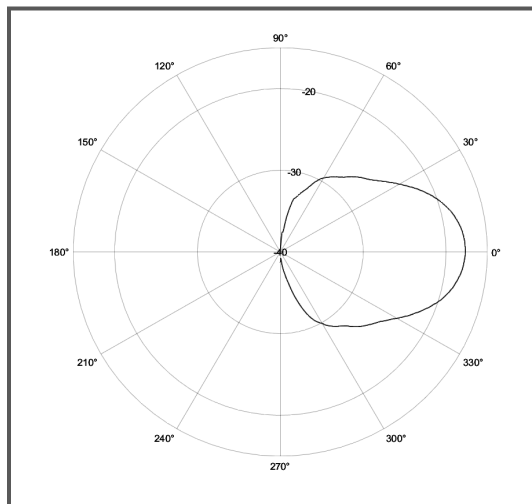


(Figure 5.9: Azimuth scan of horn antenna after modifications)

Measuring the radiation pattern of the horn antenna after adjusting the position of the face and reducing the reflectivity of the antenna mount made the radiation pattern more symmetrical and narrower. Narrowing of the emission field plot reflects a higher directivity being measured. The higher directivity represents a greater gain being measured which in turn represents a greater efficiency.

Chapter 6: Near-field to Far-field Transform

6.1 Introduction: Near-field to Far-field Transform

The near-field to far-field transform takes data that is measured in the near-field, runs it through an algorithm, and calculates the far-field factor (proportional to gain) at a specific point. A mesh of these points can then be created to calculate what the far-field gain is at each point. Then the mesh can create what the far-field radiation pattern looks like. The beauty of this algorithm is that it can be applied to any antenna test range, all that is important is the actual geometry in which the measurements are taken. This geometry is further discussed later in chapter section 6.4.

6.2 Summary of Previous Work: Near-field to Far-field Transform

As for work from previous teams, no work had been done except for a few PDF documents on information about how a transform could be done, discussing geometries and electromagnetic theories that would lead to a solution.

What exactly constitutes what the near-field and far-field relates to the frequency of operation, more specifically the wavelength (λ) of the operating frequency. The near-field is generally any region of which $r \ll \lambda$, where r is the distance from the source (antenna). So the region that is close to the source is what is considered the near-field, and in the near-field the power is “purely” reactive. While the far-field is the region of which $r \gg \lambda$, so this means the opposite of the near-field. Far-field is the region that is far away from the source and also has the property of having only radiated power. The significance of this is that the “purely” reactive power does *not* propagate while the radiated power *does* propagate; in simple terms, the radiated field carries power out radially from the source.

While one significance of the far-field being the power is carried out strictly radially, another simple reason is that many antennas operate in the far-field most of the time. Many devices use antennas to communicate wirelessly, like cell phones, satellites, AM/FM radio, etc., so being able to see how these antennas operate in these very far regions is extremely important. With that said, to confidently be in the far-field, it is generally assumed that $r > 100\lambda$. For each of the examples given, cell phones connected to WiFi at 5 GHz will have a wavelength of 60 mm. Then to be in the far-field, one would have to take measurements at a distance of at least 6 meters. At higher frequencies, it is possible to reach far-field inside a smaller ATR. However, if an FM radio antenna needs to be measured, they operate in the band of 88 MHz - 108 MHz, which gives a wavelength band of 3.4 m - 2.7 m. So to measure in the far-field, a distance of 304 m - 270 m would need to be achieved.

It can be seen that depending on the frequency of operation has a significant effect on what exactly constitutes where the far-field begins and varies drastically between different scenarios. This leads to why a transform to find the far-field becomes very important, and it is for the inside ATRs which are not big enough to reach the far-field. There are outside ATRs that can reach these large distances for measurements, but there are lots of outside factors that can give skewed readings and dirty data, such as the waves from AM/FM towers or satellites that may be

overhead or even the ambient temperature of the environment. This is why interior ATRs are much better for readings because they are in a Faraday cage which alone eliminates the outside frequencies from any source, thus the only waves inside the ATR are the ones from antennas being measured. As well as the interior is an anechoic chamber where the foam spikes are coated in a special RF absorbent which absorbs the reflected waves so the receiving antenna can only read the initial wavefront and no other reflected waves.

The CSU ATR can measure a distance of up to $\sim 2\text{ m}$, so it is very important to be able to compute the far-field when operating at lower frequencies where the far-field exceeds this distance of 100λ .

6.3 Objectives: Near-field to Far-field

There were two primary objectives with this project:

1. Convert a near-field radiation pattern into a far-field radiation pattern using a discrete computational algorithm.
2. Provide an easy-to-use software for future CSU ATR teams to transform, measure, and plot various simulated and measured electromagnetic fields.

Objective (1) needed to be completed before objective (2). The first step in the process was to verify the general functionality of the transformation, then to implement it into an easy to use software for future CSU ATR teams.

6.4 Transform

The transformation algorithm is based on a surface integral of a rectangular scan mesh. Each surface integration of these ‘near-field’ rectangular mesh produces a single point in the far-field. Therefore, in order to produce an entire far-field mesh, the surface integral would need to be swept along whichever desired axis you would want to produce a far-field mesh, i.e. along either the theta-axis or phi-axis.

$$\mathbf{E}^{\text{sc}}(\mathbf{r}) = \frac{e^{-jk_0 r}}{4\pi r} \oint_{S_1} \{ \mathbf{n}' \times [\nabla' \times \mathbf{E}(\mathbf{r}')] + jk_0 [\mathbf{n}' \times \mathbf{E}(\mathbf{r}')] \times \mathbf{i}_r \} e^{jk_0 \mathbf{i}_r \cdot \mathbf{r}'} dS'$$

(Figure 6.1: Near-field to Far-field Continuous Transformation Formula)

Given the surface integration formula supplied by Dr. Milan Ilić in Figure 6.1, different components can be separated and understood visually. This was essentially the method that Dr. Ilić himself used in order to illustrate the behavior of the transformation process for the ATR team.

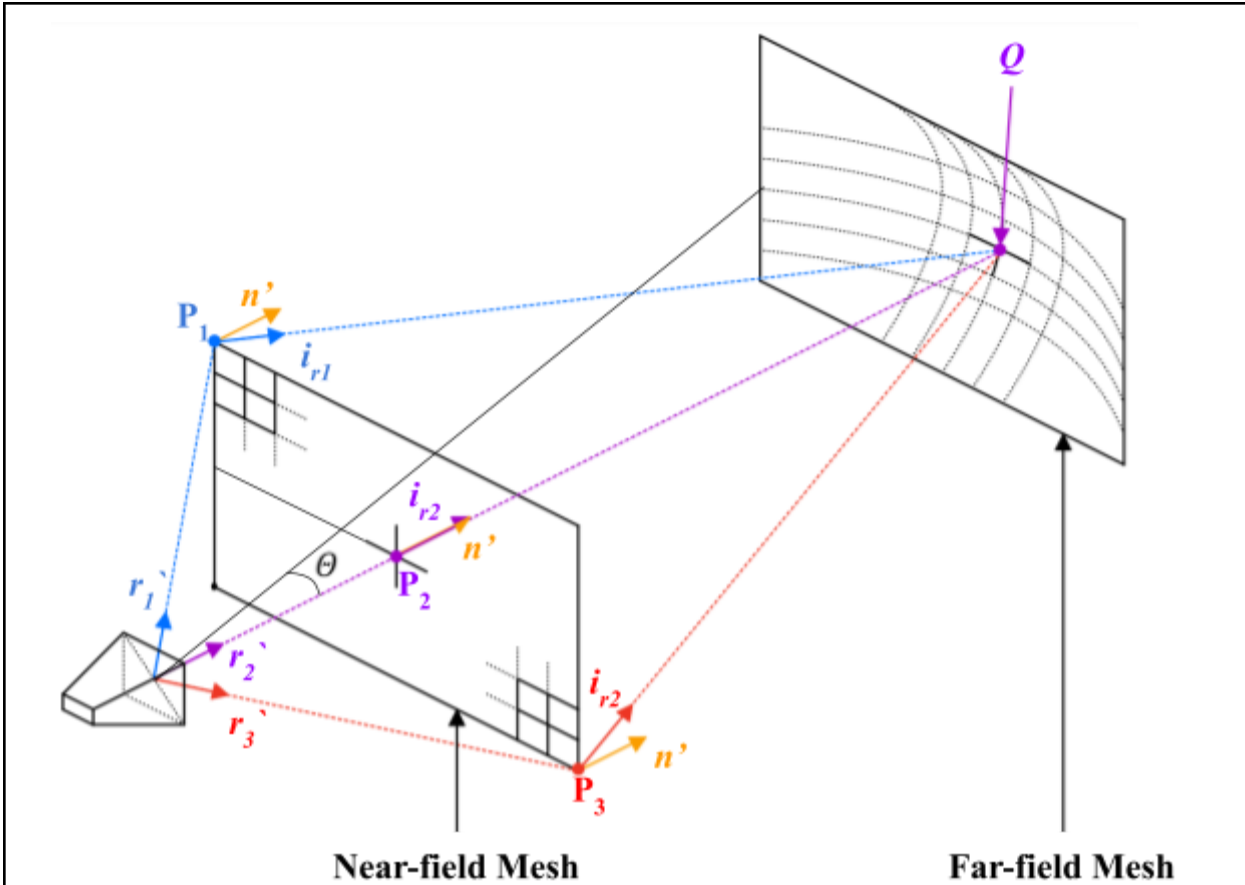


(Figure 6.2: Transformation Formula Components Visualized)

Important Visual Components	r' \equiv Unit Direction Vector to Near-field from Antenna i $\equiv i_r \equiv$ Unit Direction Vector to Far-field from Scan Point θ \equiv Angle Between Normal Vector and Far-field Point Q \equiv Central Far-field Point ($\theta=0^\circ$)
Other Components	$\nabla' \times E(r')$ \equiv Vector Field Curl r \equiv Distance from Antenna to Far-field dS' \equiv Surface Area of Scan Point K_0 $\equiv \omega/c \equiv$ Constant n' \equiv Unit Normal Vector of Scan Point

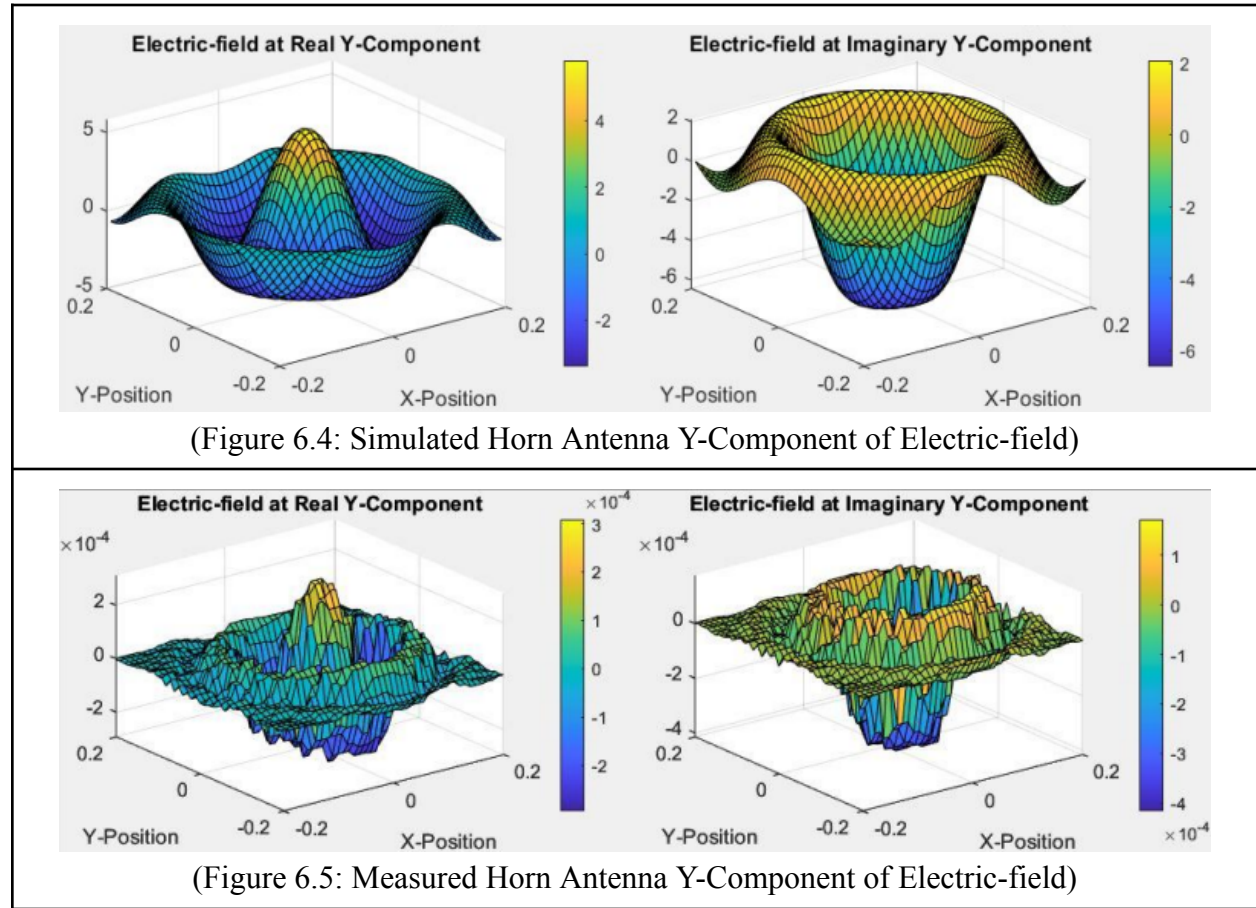
(Figure 6.3: Transformation Surface Integral Components)

As can be seen in Figure 6.2, several components listed in Figure 6.3 can be visualized. Note that in Figure 6.2, there are three reference points on the near-field mesh: P1, P2, and P3 respectively. Each of these points only represents three measured points on the near-field mesh from the VNA. Note that the r' vectors indicate the directional unit vector from the face of the ATR horn antenna to each scan point on the measured near-field mesh. Likewise, the i_r vectors indicate the unit direction vector from each scan point on the measured near-field mesh to the singular computed far-field point.

What is important to recognize about this is that on the computed far-field mesh, there is only a singular far-field point labeled Q . The entire surface integration that computes the far-field only produces one point at a time. This is because for each point on the far-field mesh, the i_r vectors change direction. Finally, note that θ represents the angle between the normal vector to a singular far-field point. In the case of Q in Figure 6.2, θ has a value of 0° .

6.5 Results

The transformation of a near-field to far-field radiation pattern was successful with a relatively small margin of error, and additionally provides some very interesting results. First, it is important to establish the verification of the transformed simulated fields of a horn antenna at 3GHz from WIPL-D. The reason for this is because the simulated fields produced by WIPL-D are much smoother, and thus produce idealized results. The difference can be seen as illustrated in Figure 6.4 and Figure 6.5.



The following is how the verification process worked:

1. Simulate a far-field distance radiation pattern to compare with a transformed far-field radiation pattern. Working at 3GHz, that places the far-field at approximately 10 meters away (see section 6.2). Any distance beyond 10 meters qualifies as the far-field.
2. Simulated a near-field radiation pattern.
3. Transform the simulated near-field radiation pattern to the far-field distance of the simulated far-field radiation pattern.
4. Measure corresponding behavior.

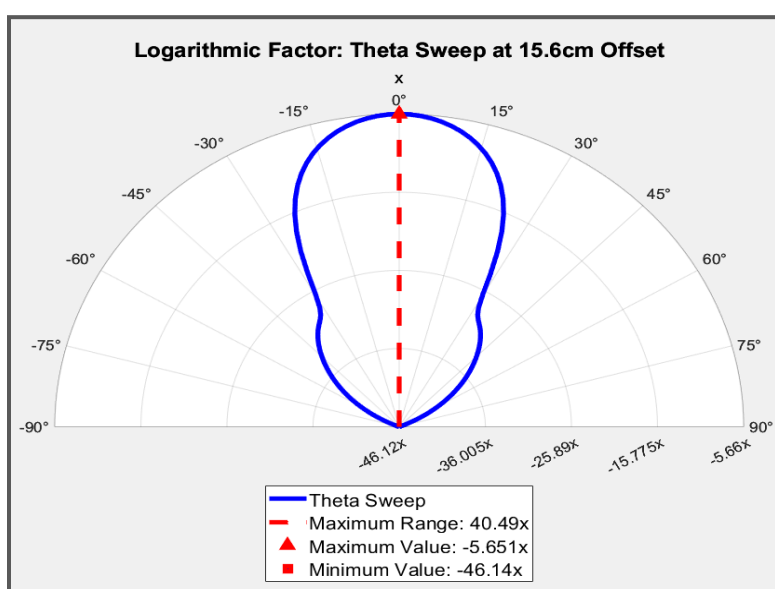


(Figure 6.6: Simulated Near-field Radiation Pattern)

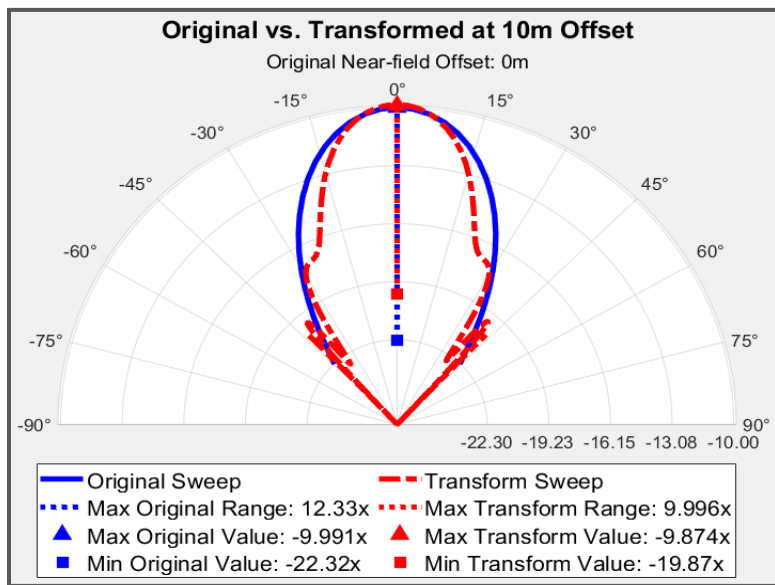


(Figure 6.7: Simulated and Transformed Radiation Pattern at 10m)

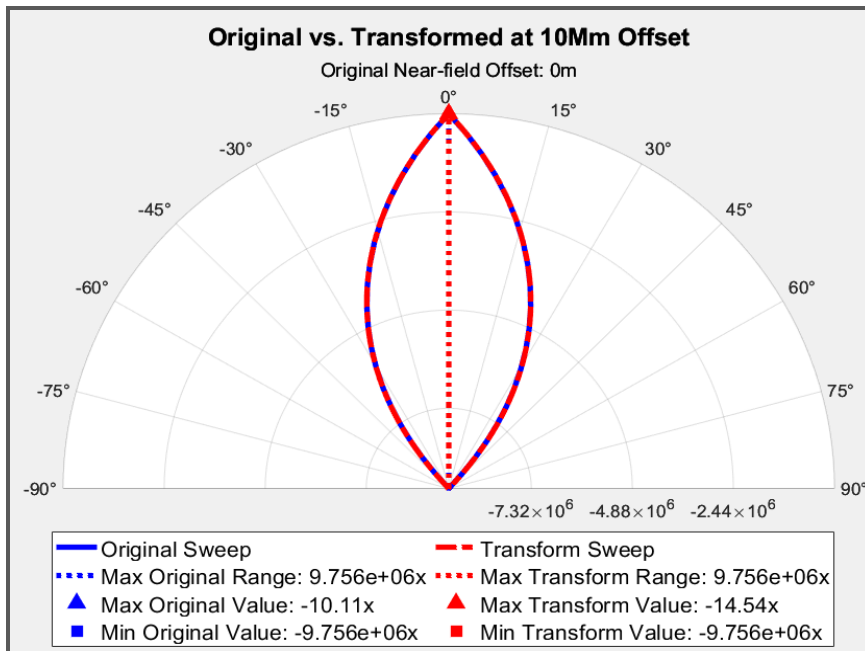


(Figure 6.8: Simulated and Transformed Radiation Pattern at 10Mm)

Measurement	10m Far-field Distance	10Mm Far-field Distance
<i>Range Error</i>	18.9%	~0%
<i>Maximum Factor Error</i>	1.17%	43.8%
<i>Minimum Factor Error</i>	11.0%	~0%

(Figure 6.9: Simulated vs. Transform Error Margins)

As can be seen from Figure 6.6 through Figure 6.9, both a transformation at 10 meters (Figure 6.7) and 10 million meters (Figure 6.8) produces a very similar radiation pattern with respect to the corresponding simulated field at the same far-field distance. An interesting observation is that the further the far-field distance, the more accurate the transformation becomes. This can be seen in Figure 6.9. At a far-field distance of 10 million meters, despite the maximum factor value producing an error margin of approximately 43.8%, the transformed range and minimum value are nearly identical. What makes the radiation pattern itself significant is not what the maximum or minimum values are so-to-speak, but how the radiation is distributed across space. More simply, what the ‘shape’ of the radiation is.

Given this information, and confirmation from Dr. Milan Ilić, the near-field to far-field transformation algorithm works within a relatively small margin of error.

6.6 Software

Regarding objective (2) from section 6.3, we were successful in making a function MATLAB based software intended to be used by future CSU ATR teams in an effort to provide subsequent ATR teams with the ability to transform their own near-field radiation patterns to far-field radiation patterns. With that stated, the software is far from flawless, and does little in the way of error checking. However, it should provide future ATR teams with a beneficial tool for far-field radiation modeling.

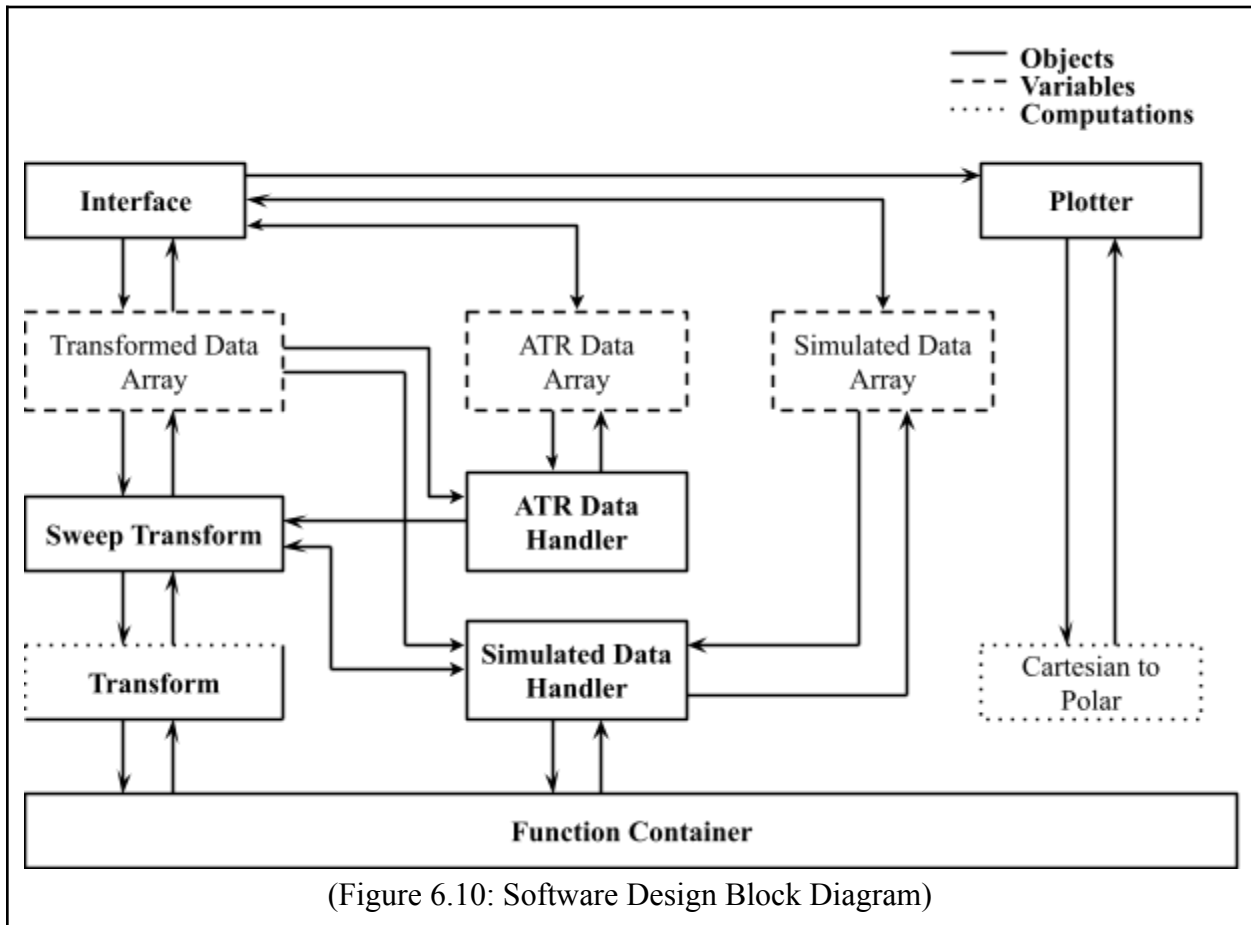


Figure 6.10 illustrates the general behavior of the software, and includes objects, computations, and important variables and how they all intercommunicate. The software itself can be run with a simple executable, labeled ‘NFtoFF.exe’. In the same directory, there should exist both a ‘Data’ folder and a ‘MATLAB Source Files’ folder. The former folder contains all of the MATLAB objects and the main file.

This software can be found on the ATR PC, ATR 2022/2023 Google Drive folder, and in the CSU Antenna Test Range Trello page.

6.7 Software Capabilities

The software ‘NF->FF’ designed to do the following:

1. Transform Simulated or ATR Scanned EM Fields
2. Store Simulated or ATR Scanned EM Fields for comparison
3. Plot
 - a. Polar Field Strengths
 - b. Cartesian Field Strengths
 - c. 2D & 3D Heatmaps (Near-field X,Y, and Z components only)
4. Plot both a linear and a logarithmic factor (proportional to gain) of field strength

6.8 Notable Observations

Approximate Curl

- The curl aspect of the transform surface integral as mentioned in Figure 6.3 can be approximated as using the electric-field. However, a more exact curl can be derived from the magnetic-field. This is possible with simulated data with WIPL-D, and so NF->FF provides the user an option to approximate curl. However, the use of the magnetic-field to produce the exact curl is not yet possible with the ATR.

Approximate Curl Computation	Exact Curl Computation
$\nabla' \times E(r') \approx -j \cdot k_0 \cdot i_r \times E(r')$	$\nabla' \times E(r') = -j \cdot \omega \cdot \mu_0 \cdot H(r')$

(Figure 6.11: Approximate and Exact RF Wave Curl Computation)

Surface Area Adjustment

- As seen in Figure 6.3, the discretized version of the surface integral requires each discrete computation to be multiplied by the surface area the point in the rectangular mesh occupies. However, the rectangular mesh that is transformed only covers approximately $\frac{1}{6}$ of the total surface surrounding the transmission antenna as seen in Figure 6.2, the surface area needed to be multiplied by six. However, for an undiscovered reason, multiplying by five produces better results.

Far-field Distance and Accuracy

- As previously mentioned, the relationship found was that the further the far-field point is set, the more accurate the radiation pattern is. This is because of the effect that the directional vectors, r' and i_r , have in relationship to the surface because less and less apparent the farther the far-field point is made. This can be seen in Figure 6.12 and Figure 6.13.

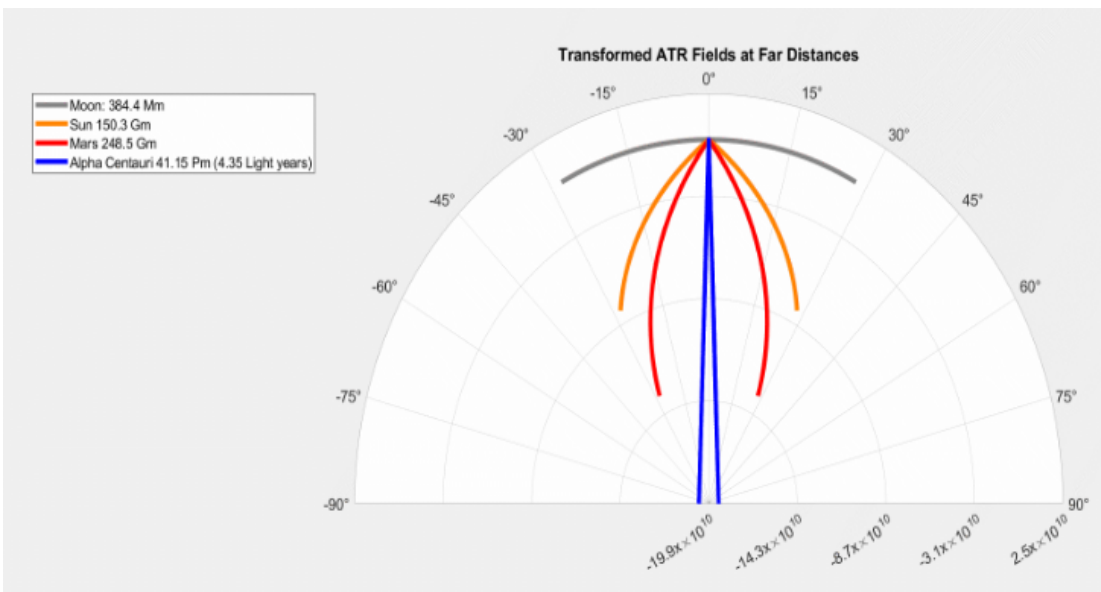


(Figure 6.12: ATR Transformed Far Distance Far-fields)

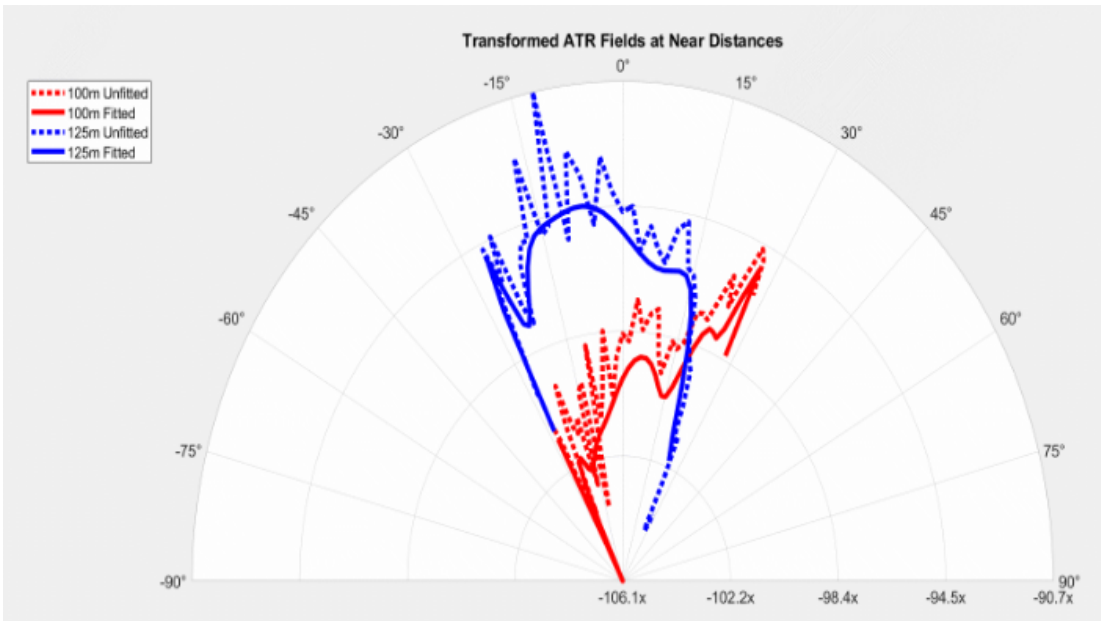


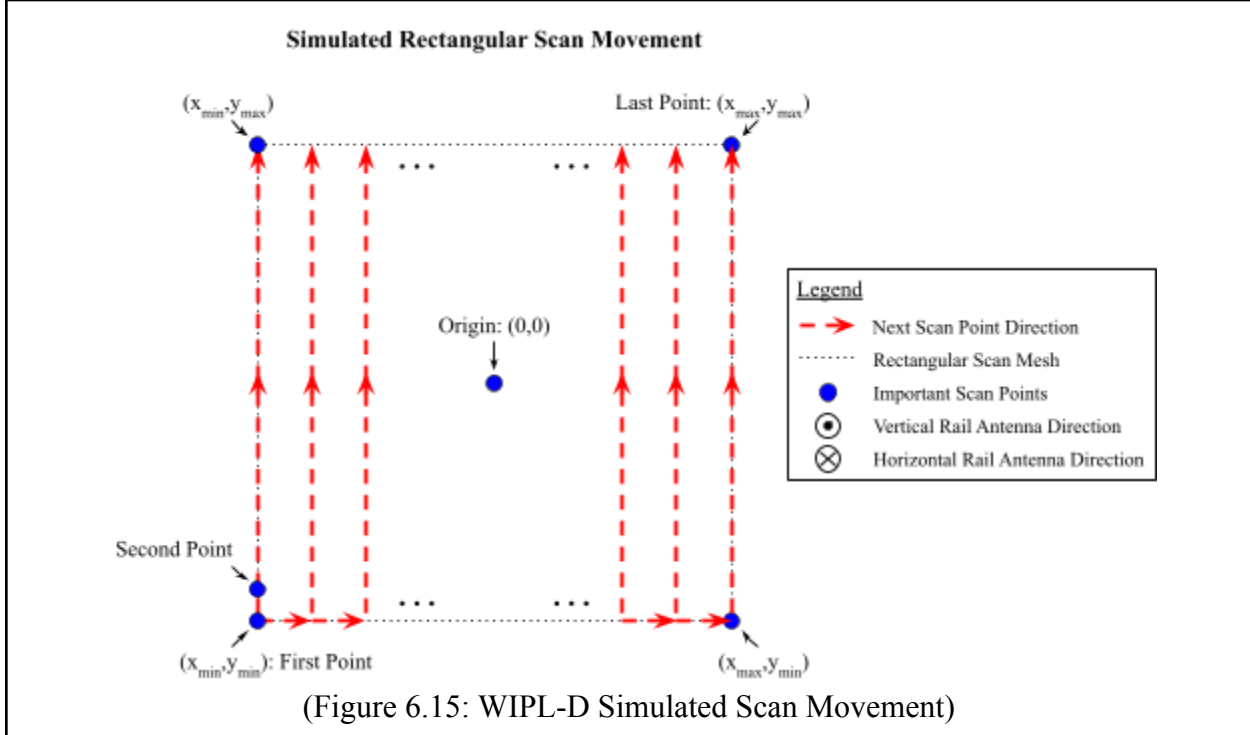
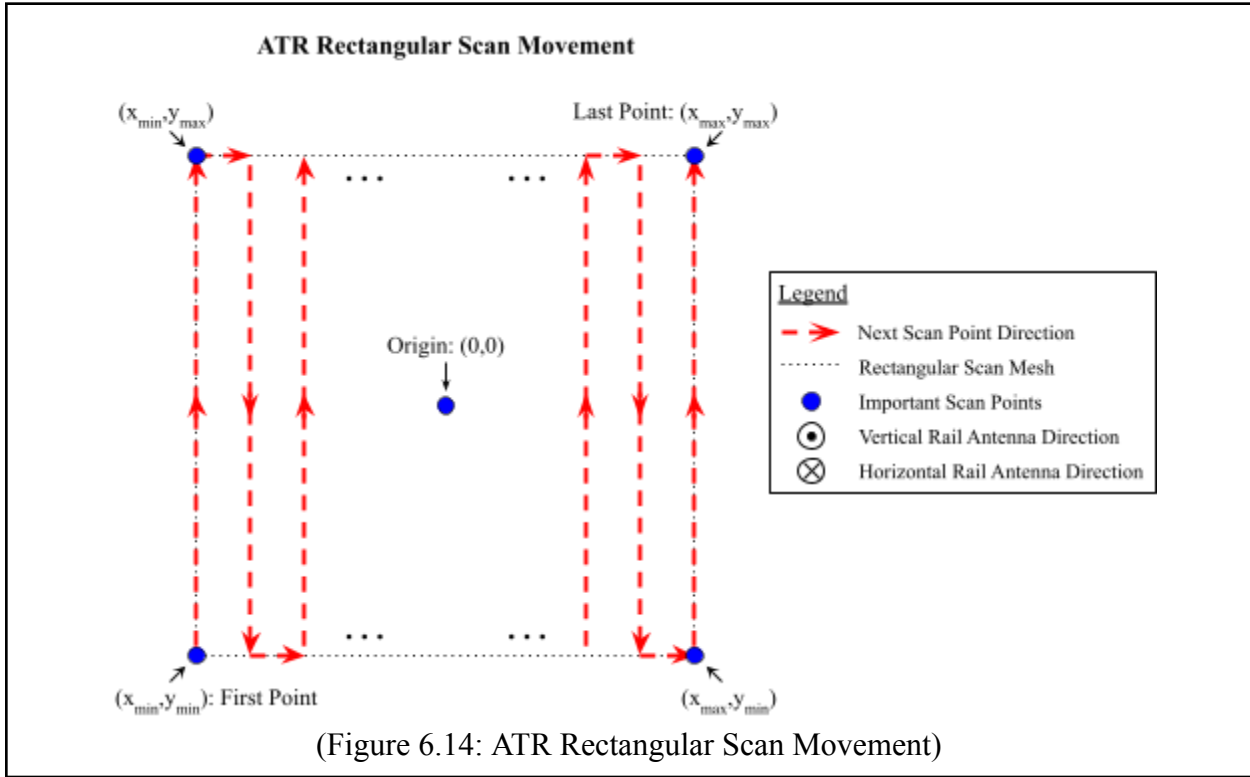
(Figure 6.13: ATR Transformed Near Distance Far Fields)

Polynomial Regression Line Fitting

- As seen in Figure 6.13, when the far-field point is not far enough, the result is very poor (red line). However, as the far-field distance increases, the results become better (blue line). In order to give us a better approximation, polynomial regression line fitting was used to create lines of best fit that better represented what the radiation pattern should look like. This can be seen with the solid lines in Figure 6.13.

EM Field Data Storage

- The way in which simulated data and data obtained from the ATR orders itself is vastly different. This is why there are two separate object files that parse the data obtained from both simulated and measured sets. Figure 6.14 and Figure 6.15 illustrates this.



Chapter 7: 5-Element Patch Antenna Array

7.1 Goals of Design

A design of a patch antenna array consisting of 5-elements will be designed with the intent of measuring and characterizing the device using Colorado State Universities Antenna Test Range. This array is not being designed with the intent of adding it to any device or used in any communication system, it is strictly designed for academic purposes and proof of knowledge. The first goal of this patch antenna is the physical size, it is desired for the final PCB to have dimensions less than $15\text{ cm} \times 15\text{ cm}$, be fed by a total of five SMA connectors with an impedance of $50\text{ }\Omega$, and have a maximum gain greater than 12 dB .

7.2 Background Information

A five-element patch antenna array consists of two different ideas, the first being the patch itself and the second comes from lining up n amount of these antennas which is called an array. The idea behind how a patch antenna works will be discussed and then the significance of adding them into an array.

First off, a patch antenna works on the same idea behind a normal dipole antenna where an alternating current is fed to it (this current is usually carrying data) and due to the alternating current (which in turn alternates the voltage/charge) will radiate an electromagnetic wave. And this electromagnetic wave carries power outwards from the antenna which can then be received by another antenna. Where a patch antenna differs from a dipole antenna or any antenna is the physical form of it, normally a dipole antenna is a straight wire with some length, or a horn antenna uses a monopole (or multiple) with a metal horn whereas a patch antenna is built with a printed circuit board (PCB) where there is a patch island above a ground plane. And this patch island above the ground plane alternates voltage/charge and generates an electric field. While most of the electric field is located between the patch and ground plane, there is a phenomenon called fringing where the electric field begins to bend out from between the patch and ground plane.

Another important characteristic of different types of antennas is their radiation pattern, and this pattern is unique to the physical shape of the antenna and the frequency at which it operates. However, we will not be going into excruciating detail of how to find these radiation patterns, but it is important to know they exist and have significance. For instance, a normal radiation pattern of a patch antenna is shown in figure 7.1 and it simply shows the direction of which the antenna will propagate a wave the best with highest gain (or worse with lowest gain). And if two different patches have the same parameters, as in length and width, they will exhibit the same radiation pattern. But in the case of a patch antenna, it can be seen that it has a very broad radiation pattern which means that it can radiate to a wide angle.

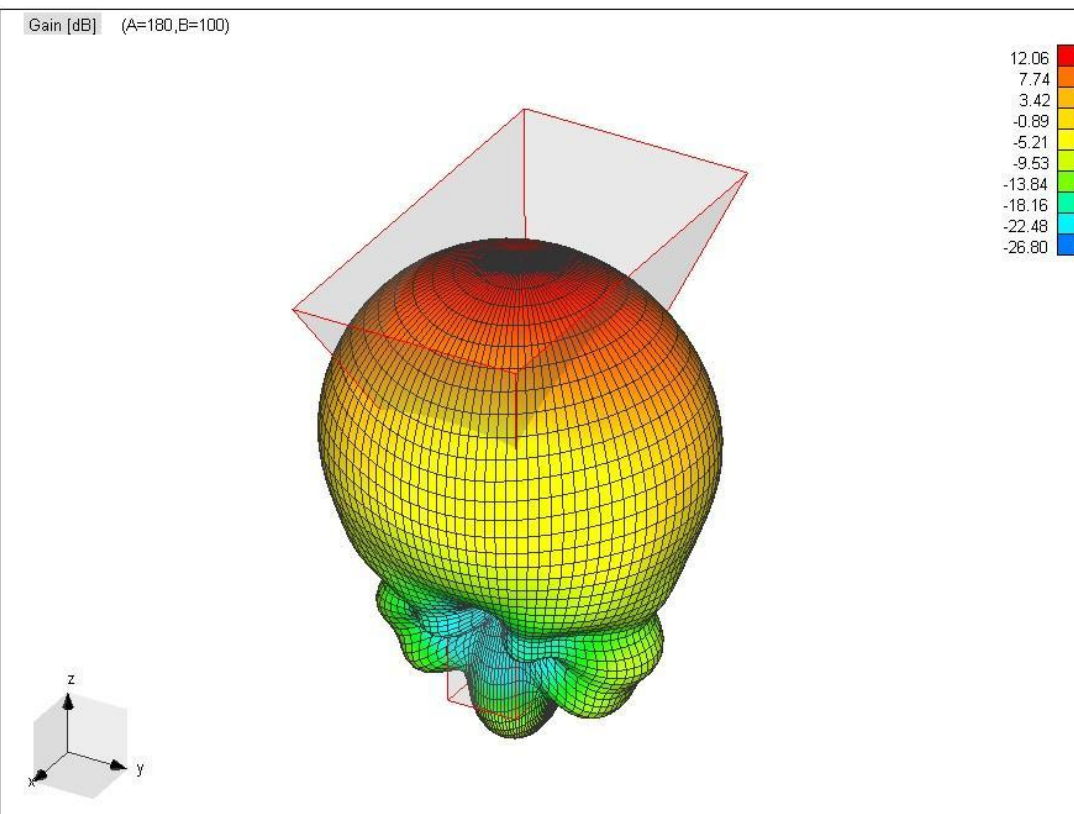


(Figure 7.1: Radiation pattern of a horn antenna generated in WIPL-D)

Secondly, as discussed earlier, each patch will have its own radiation pattern with the patch antenna having a very broad radiation pattern. But what if we want to use patch antennas but have a much more directed main lobe, so as to make it not as broad? Well, that is where putting them into an array can become very useful. Adding antennas in an array can change their radiation pattern by using constructive and destructive interference. Generally, each antenna is placed $\frac{\lambda}{2}$ apart which can give two different base cases depending on the phase of the signal fed into the antenna. In the case that the antennas are fed *in-phase* will result in a main lobe that is normal to the array axis and is called *broad-side*. In the other case, the antennas are fed in *counter-phase* which will result in two main lobes that are parallel to the array axis and is called *end-fire*. By adding more antennas into the array, it will increase the gain of the main lobe (since more antennas are contributing to it) and at the same time make it even more directed. With the use of antenna arrays, a *very* narrow main lobe can be generated, and this can be very useful in many places such as radar and deep space communications. These arrays are not only confined to a single axis, multiple rows and columns can be used and this will allow even more control over the beam. Then add the control of the phase of each of the antennas, then you can create something called an electronically controlled phase-array and that allows for the beam to be actively controlled instead of having it at set position.

7.3 Calculating lengths of patch and position of rear-feed line

Calculating the lengths of the patch antenna are directly related to the wavelength of the operating frequency. In an ideal situation, the length of the patch will be half of the wavelength. However, in the real world the ideal situation is not applicable, so the fringing effect is taken into account, and this will alter the length and width of the patch beyond the half wavelength.

Before any calculations can begin, there are a few constants that need to be defined, such as the dielectric permittivity and resonant frequency. In the case of this patch, the dielectric is selected to be the commonly used FR4 and has a permittivity of $\epsilon_r = 4.3$ (this is an average, typically it ranges between $3.8 \leq \epsilon_r \leq 4.8$). The resonant frequency was selected to be

$f = 10 \text{ GHz}$, and there are a few reasons this was selected. The main reason is due to the fact that the antenna test range uses a horn antenna as the receiver and it operates in the X-band, so the patch needs to operate in the same frequency band. The second reason is since the size of the patch and patch separation is directly related to the wavelength, a lower frequency (larger wavelength) would result in a larger patch, and the patch was desired to be small. The last constant that needs to be defined is the height of the dielectric, this height is determined by the standard height of PCBs. The preselected company of choice that this antenna will be manufactured by is Advanced Circuits located in Aurora, CO. The standard two-layer PCBs have a height of $h = 1.57 \text{ mm}$.

The first of the patch is found using [4]:

$$W = \frac{c_0}{2f} \sqrt{\frac{2}{\epsilon_r + 1}} = \frac{299,792,458 \frac{\text{m}}{\text{s}}}{2(10 \text{ GHz})} \sqrt{\frac{2}{4.3 + 1}} = 9.2144 \text{ mm}$$

$$W = 9.2144 \text{ mm}$$

Before finding the length, the effective permittivity needs to be found. This effective permittivity comes from the fringing effect since some of the electric field will be in air and some inside the dielectric. The effective permittivity is found using [4]:

$$\epsilon_{ref} = \frac{\epsilon_r + 1}{2} + \frac{\epsilon_r - 1}{2} \left[1 + 12 \frac{h}{W} \right]^{-\frac{1}{2}} = \frac{4.3 + 1}{2} + \frac{4.3 - 1}{2} \left[1 + 12 \frac{1.57 \text{ mm}}{9.2144 \text{ mm}} \right]^{-\frac{1}{2}}$$

$$\epsilon_{ref} = 3.595$$

Now that the width and effective permittivity has been found, the length needs to be calculated. The length will have two parts, the first part is the main length (L_m), but since fringing is taken into effect, an additional length (ΔL) needs to be added. The length of the patch is found using [4]:

$$L_m = \frac{c_0}{2f \sqrt{\epsilon_{ref}}}$$

(31)

$$\Delta L = 0.412h \frac{(\epsilon_{ref}+0.3)(\frac{W}{h}+0.264)}{(\epsilon_{ref}-0.258)(\frac{W}{h}+0.8)}$$

↓

$$L = L_m - 2\Delta L = \frac{c_0}{2f\sqrt{\epsilon_{ref}}} - (2)0.412h \frac{(\epsilon_{ref}+0.3)(\frac{W}{h}+0.264)}{(\epsilon_{ref}-0.258)(\frac{W}{h}+0.8)} = \frac{299,792,458 \frac{m}{s}}{2(10 \text{ GHz})\sqrt{3.595}} - 0.824(1.57 \text{ mm}) \frac{(3.595+0.3)(\frac{9.2144 \text{ mm}}{1.57 \text{ mm}}+0.264)}{(3.595-0.258)(\frac{9.2144 \text{ mm}}{1.57 \text{ mm}}+0.8)}$$

$$L = 6.519 \text{ mm}$$

Finally, the feed point (y_0) of the patch antenna needs to be found. Also note that since the patch will be fed using a 50Ω SMA, the input impedance will also be 50Ω . The feed point can be found using [4]:

$$G_1 = \frac{1}{120\pi^2} \int_0^\pi \left[\sin\left(\frac{k_0 W}{2} \cos \theta\right) \right]^2 \theta d\theta = 0.0011$$

$$G_{12} = \frac{1}{120\pi^2} \int_0^\pi \left[\sin\left(\frac{k_0 W}{2} \cos \theta\right) \right]^2 J_0(k_0 W \sin \theta) \theta d\theta = 0.0006641$$

↓

$$y_0 = \frac{L}{\pi} \arcsin \left(\sqrt{2R_{in}(G_1 + G_{12})} \right) = 2.5178 \text{ mm}$$

$$y_0 = 2.5178 \text{ mm}$$

Where: k_0 is the wave number

R_{in} is the input impedance $\sim R_{in} = 50 \Omega$

J_0 is a Bessel function of the first kind of zero order

The last thing to do is to find the minimum size of the ground plane that needs to lie under the patch on the PCB. But this is generally $W + 10h$ or $L + 10h$.

$$W_g = W + 10h \rightarrow W_g = 24.96 \text{ mm}$$

$$L_g = L + 10h \rightarrow L_g = 22.26 \text{ mm}$$

With W , L , y_0 , and the ground plane found dimensions, the design of the patch is now complete.

(32)

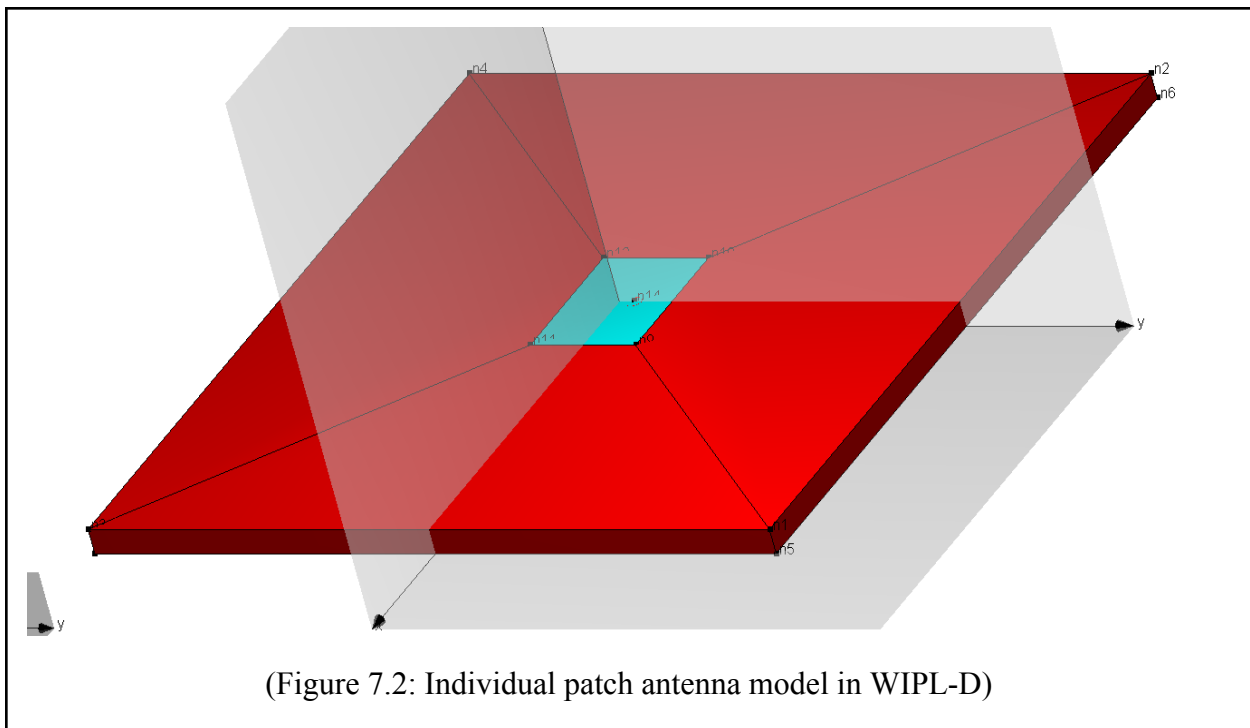
7.4 Simulation

In order to fully develop the 5-element patch antenna array, a single patch antenna would need to first be simulated. Following a successful simulation of a single patch antenna, an entire array of patch antennas could be developed and simulated.

7.4.1 Simulation of patch antenna

With the initial dimensions of the patch found, it is time to throw them into simulation software to see the radiation pattern of the individual patch. The software that was selected to simulate the patch (and later the array) was WIPL-D, which is a software program that is excellent for simulating radiated antenna fields. In fact, the advisor of the CSU ATR, Branislav Notaros, was on the development team for the software.

It is important to note that the patch is simulated on a finite ground plane and not an infinite one because when it comes to the edges of the plane, they are within a close enough distance that infinite cannot be assumed. This patch can be seen in figure 7.2 where the red signifies the dielectric and the teal signifies the conductor, or patch. In the center of the patch, it can be seen that the voltage generator is located to the right of the origin, this signifies the feedline of the patch. The frequency of the input for the simulated radiation was at 10 GHz and the radiation pattern can be seen in figure 7.3.



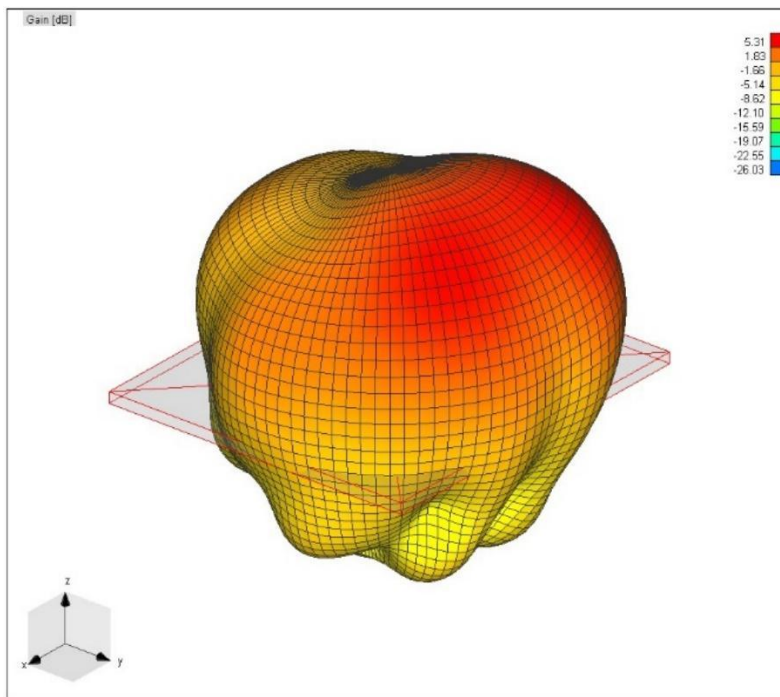


(Figure 7.3: Radiation pattern of patch antenna)

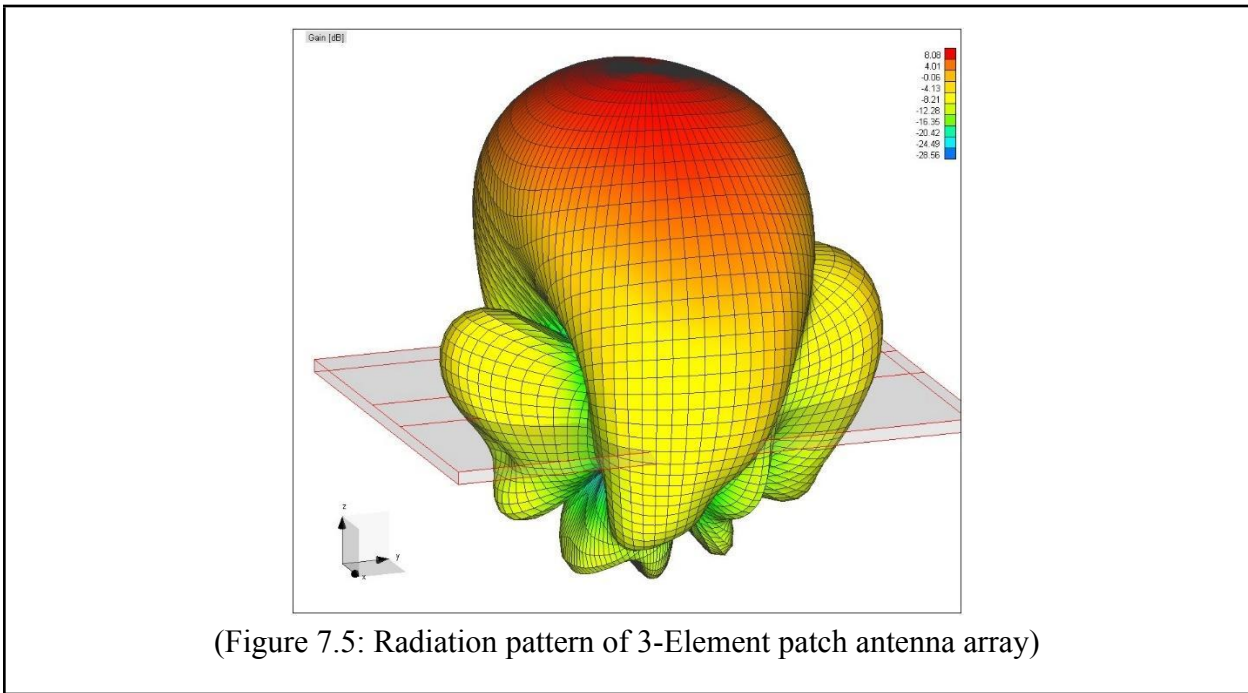
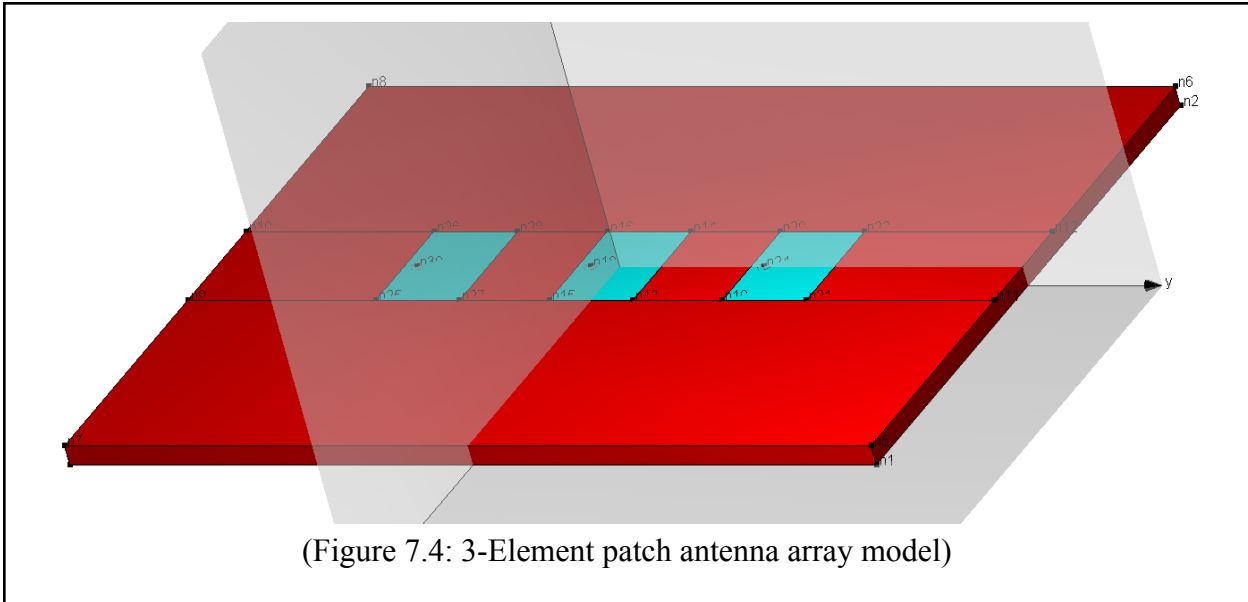
The radiation pattern has a good general shape which has a wide higher gain region normal to the patch radiating with a higher gain. The individual patch has a peak gain of 5.31 dB which is slightly lower than the typical patch antenna, but it is still acceptable in terms of this project.

Now that the individual patch has been simulated and produced acceptable results in terms of the radiation pattern and gain, it is time to move onto simulating the patch in a 5-element array.

7.4.2 Simulation of 5-element patch antenna array

The software to simulate the 5-element patch antenna array is still WIPL-D and all the meanings of the colors have remained the same. It is important to note again that the separation between the edges of the patches is $\frac{\lambda}{2}$ and this is allowing the array to have a broadside radiation, in other words the radiation will have a maximum gain normal to the ground plane. Two key characteristics of throwing the patches into an array is that the radiation pattern will become more directed and maximum gain of the main lobe will increase.

Before 5 elements were tested, a 3-element array was created just to see how the array radiates and if two things happen. First, if the general shape of the radiation pattern becomes more directed and if the gain of the main lobe increases. The 3-element array can be seen in figure 7.4 and the radiation pattern in figure 7.5.



The radiation pattern shows the two trends that is desired, with both the radiation pattern becoming more directed to the broadside and the gain has now increased to 8.08 dB . Since this trend is desired, it was acceptable to add the final two patches for the desired 5 elements. The 5-element patch array can be seen in figure 7.6 with its radiation pattern shown in figure 7.7 and 7.8.

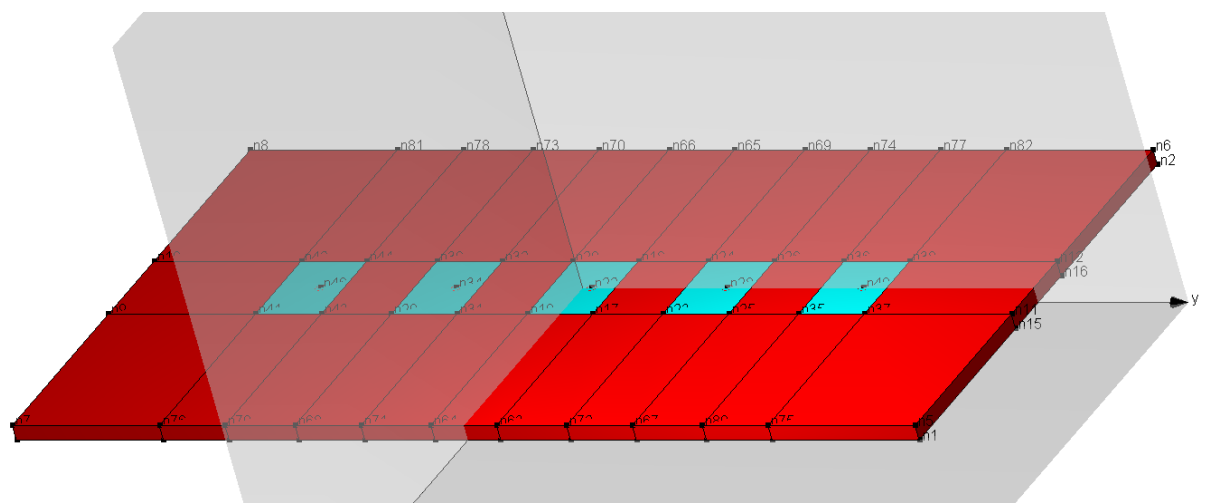


(Figure 7.6: 5-Element patch antenna array model)

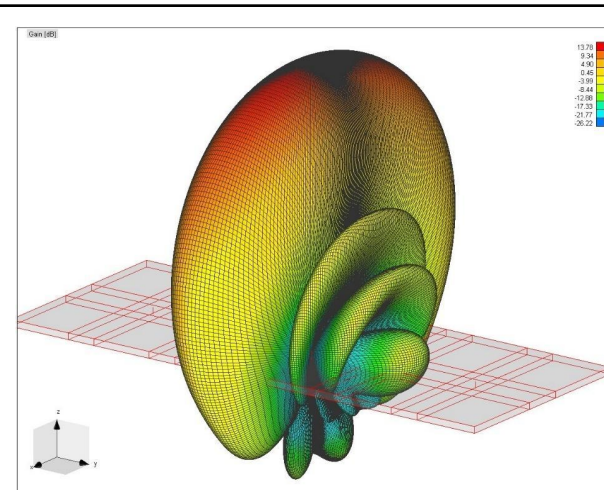


(Figure 7.7: 3-D Radiation pattern of 5-Element patch antenna array)

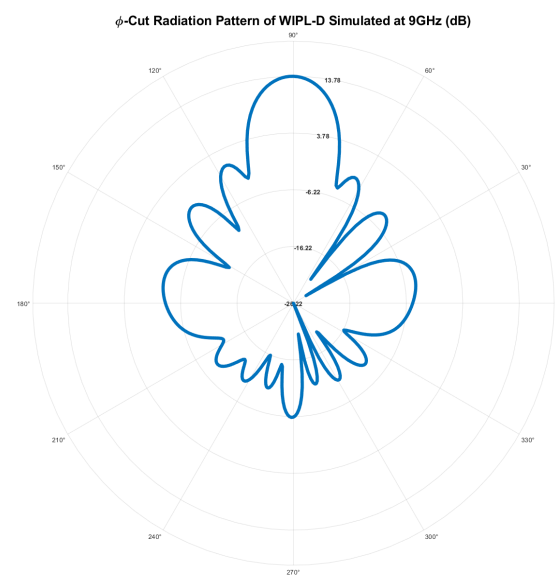


(Figure 7.8: ϕ -cut Radiation pattern of 5-Element patch antenna array)

The maximum gain has increased all the way to 13.78 dB which has exceeded the goal of 12 dB and the main lobe has become very directed with a few side lobes. These side lobes are not as desired, but they are hard to avoid when adding them into an array. But nonetheless, the simulated radiation pattern for the 5 elements is acceptable and therefore the design to produce the patch antenna can begin.

7.5 Generating Gerber Files for PCB

Now that simulation of the patch antenna array is complete and showing adequate results, it is time to move onto the manufacturing of the patch antenna array. The software used to design the PCB was KiCad and it was decided to run the feedlines on the same plane as the ground plane and this was to mitigate the crosstalk between the lines. Another important design parameter is the trace that connects the SMA to the via was designed to have an impedance of 50Ω to continue to match all the impedances. The overall design process of the PCB was simple as the whole array has already been designed and it was a matter of just getting it replicated in KiCad to be sent to some manufacturer. The PCB can be seen in figure 7.9. The PCB had the specifications that the dielectric is FR-4, two layers, and it is $\sim 2.4'' \times 5''$. The manufacturer that was selected was Advanced Circuits since they were a local company and had been recommended by various engineers.

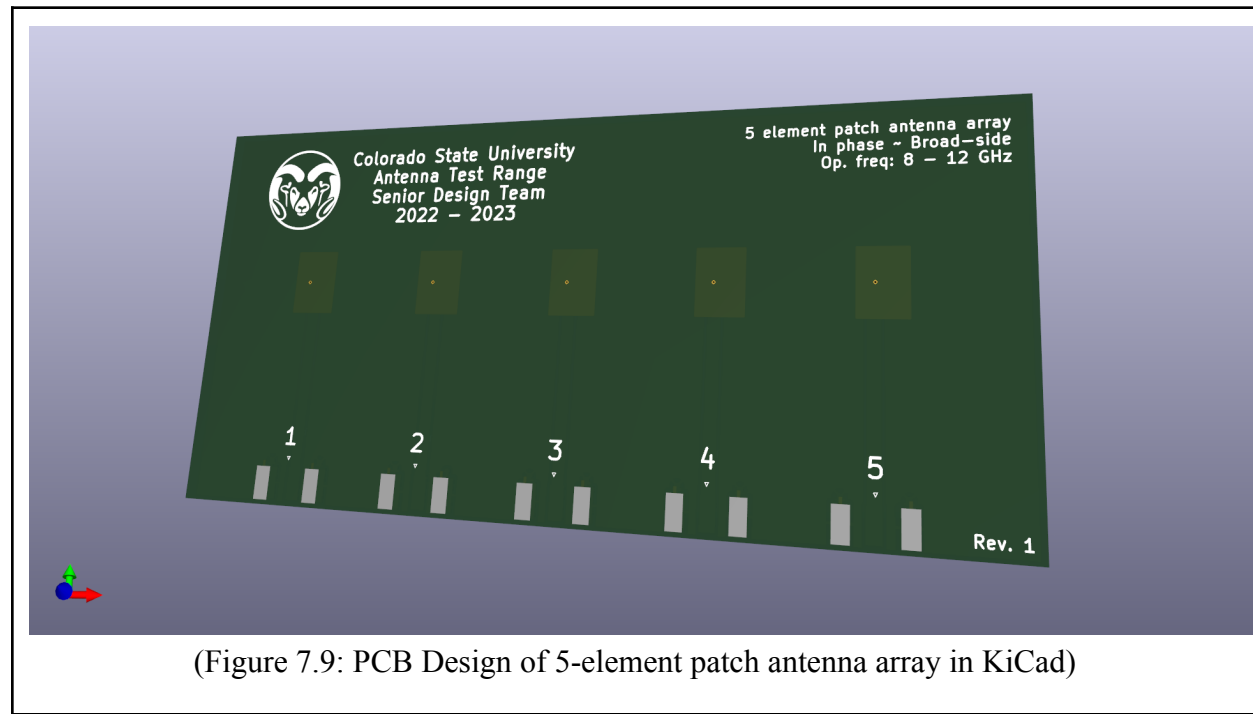


(Figure 7.9: PCB Design of 5-element patch antenna array in KiCad)

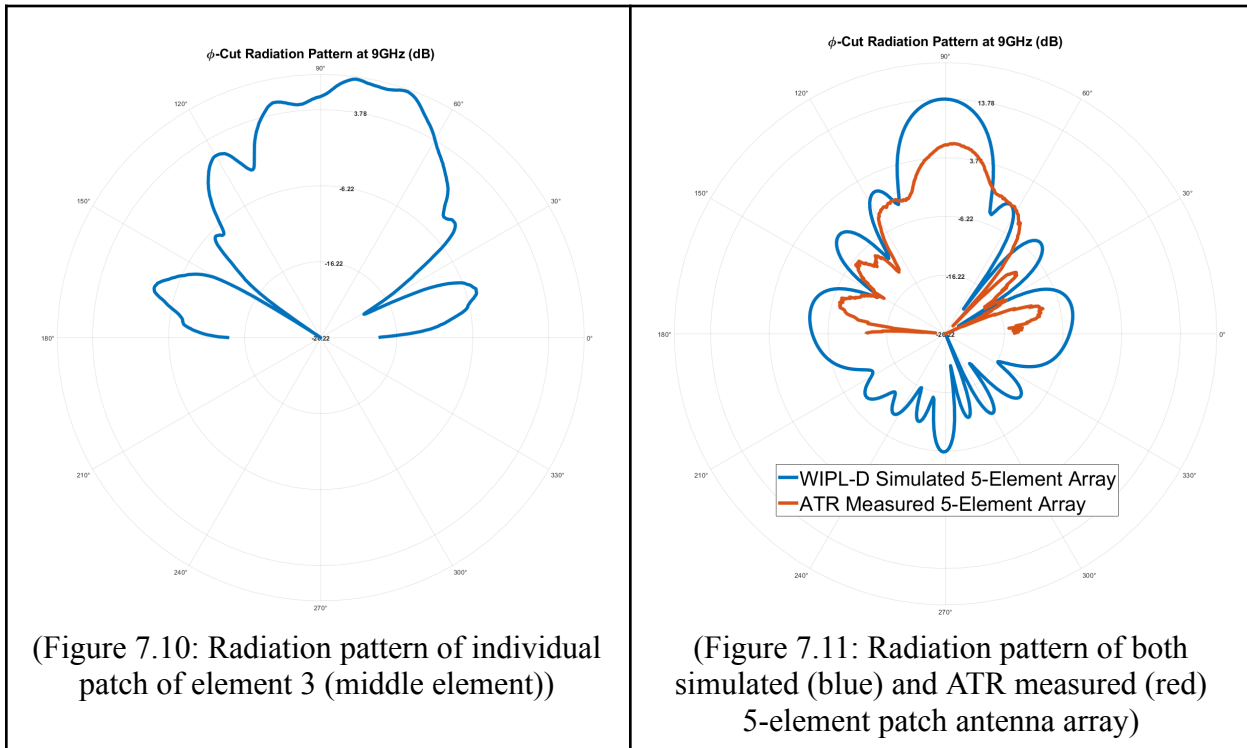
7.6 Antenna Test Range Measurements

With the antenna in hand, some additional work with the mechanical engineers on the team needed to be done to get a mount for the patch antenna (which was discussed in previous sections). And after the mount was created, the antenna was able to be put into the range and measurements made.

The geometry that was measured was a 180° sweep of the azimuth direction, this was done because it shows the most nulls and lobes, seen above in figure 7.8. The method of measuring the antenna consisted of making 5 separate measurements, which meant hooking up each coaxial cable to each port on the patch antenna and making a measurement of the single patch. Each scan of each patch was done from 7GHz to 13GHz to cover the entire X-band and a little bit more. Once the 5 measurements were made, they were exported and by using Matlab,

the 5 fields were all superposed on top of one another. This is perfectly okay to do instead of taking a single measurement with all 5 patches fed at the same time as superposing the individual fields on top of each other is identical.

Looking below at figure 7.10, which is one of the 5 separate patch measurements, it can be seen to have a broad main lobe with two smaller lobes. And then figure 7.11 shows the total radiation pattern (red line) of all 5 elements superposed on top of each other and the simulated field from WIPL-D layered on top to help compare both fields. Looking at the nulls between both of them, they both line up in the same spots and both resemble each other which is a great sign and gives enough proof to affirm that the patch antenna array is a success and met the objectives.



7.7 Wrapping It All Up

The end goal of designing the antenna had two objectives, to gain experience designing and testing an antenna, but to also use the antenna test range for what it is used for. The process of initially designing the antenna with different specifications gave insight into what all needs to be thought about before the design process can begin. Such as the material that will be used, height of the dielectric (since the height can change the radiation pattern), the phase at which the patches will be fed, and even how the feedline will supply the antenna. Moving onto the simulation, there are many different parameters that need to be accounted for and what about the radiation pattern is desired and what is deemed good or bad. And working in KiCad, it also was a whole process with the vias, traces, and planes. It was very important to know which conductors

are connected to which ones and that it would not be good to connect the feed trace to the ground plane. And finally with getting the measured fields from the antenna test range, it took knowledge of electromagnetics to know that each patch can be measured and then superposed on top of each other to get the total radiation pattern.

There is some discrepancy between the simulated and measured radiation pattern, and these can stem from a few things. The first being that the simulation works with ideal conditions such as perfect electric conductors and no losses. A big difference between the simulation and the real PCB is that in WIPL-D, the traces could not be considered and that the generators were connected directly to the patch where the via's are located. This would eliminate any possible crosstalk. Another consideration is from human error and when the measurements are being taken, they are of each individual patch so the whole scan needs to be reset each time. And there is a chance that the location of each can is not at the exact same location and that instead of superposing a single point, it is superposing a small area where 5 different elements were scanned. Both could lead to discrepancies between the simulated and measured radiation pattern. But again, they both resemble each other very closely with the nulls lining up perfectly except the two in the main lobe.

Chapter 8: Standards

The primary IEEE standard that has been used is IEEE standard 149-2021 which is the *IEEE Recommended Practice for Antenna Measurements*. It describes that the fundamental property of any antenna is its radiation pattern, and the different parts of the radiation pattern are the magnitude/phase, gain and directivity, polarization, radiation efficiency, and impedance [2]. This standard applies to the CSU ATR because it states that the fundamental property of any antenna is the radiation pattern and that is exactly what we are measuring. Using the radiation pattern can give the different aspects of the field at a point, such as the magnitude and phase, which is mainly what the CSU ATR does, it measures the real and imaginary part of the field.

Chapter 9: Conclusion

The 2022-2023 CSU ATR team's main objectives has been a challenge given little knowledge of how the ATR operates, so this term has had a primary focus on improving the physical operation of the ATR. The team overcame the challenges together and made good progress on improving different aspects of the ATR.

A critical fix that has been pursued was the antenna mount because this will fix the issue of the horn antenna sitting in front of the φ -axis, instead of the origin. Two additional perks of this fix has been that it will allow the ATR to mount various antennas of different shapes and sizes and allow the MRI team to use the ATR to make measurements for their own senior design project. The MRI aspect of this fix has been implemented and been working well as their team has been able to conduct their own readings by using the mount and running scans. This will further continue into the next term to refine the appearance of the mount and functionality of the elevation motor.

The redundant store and server integration has shown to be very useful as all the readings can now be stored in a single location for all current and future users to access, as well as backup readings in the worst case scenario where they get lost, deleted, or corrupted. This upgrade has shown to be a big success as the storage has been used to store readings which all can access, including Arduino code for the remote switch.

The motor controller case initially had a good design that would supply adequate cooling, decrease the footprint, and give the components more protection. However, further on in the semester, the objectives with the case had changed because the ATR is a great educational tool for introducing antennas and electromagnetic concepts to those who are not familiar. The open layout where all the different components can be seen well was determined to be an interesting viewpoint for these tours. Therefore, the new designed motor controller case was not implemented and will not continue into the next term. However, the remote switch, which is part of the case, has been implemented and allows the user to turn on the motor controller remotely from the computer by running an Arduino code and this has been seen to be a success as the user can now remotely turn on the motor controllers.

The 5-element patch antenna array was selected for two reasons, to use the ATR for testing a new antenna that has never been built before and to allow the students to use knowledge from CSU to build and design an antenna. The project provided a lot of insight into the process of designing an antenna. From the beginning stages of research to the final testing, the patch antenna has had successes throughout with achieving a high gain patch antenna to a higher directivity array. In the end, once the array had been put into the ATR, it produced a radiation pattern that matched nearly identically to the simulated field showing the success of the design and the antenna.

Finally, the near-field to far-field transform has been a challenging development of electromagnetic theory and computational electromagnetics. But in the end, the task of designing an algorithm to compute the far-field from the near-field has proved successful. Though it cannot yet be concluded how beneficial it will be, we hope that future CSU ATR teams will endeavor to continue to improve this software.

Chapter 9: Future Work

9.1 Future Work: Motor Controller Case and Upgrades

The current motor controller case has many benefits but still requires future work. Environmental hazards still cause a potential risk for damaging the hardware mounted on the board. The current design is optimal for demonstration purposes, thus future teams would need to consider a solution for creating a case that can optimize the air flow over the motor controller boards while still having the potential for being used for demonstration. Additionally, the device must also optimize the space constraints caused by the desk. However, it is not necessarily crucial to the operation of the antenna testing range, thus other projects related to decreasing the wait time before each scan should be prioritized in terms of mechanical functions. In terms of the motor controller upgrades performed the boards will likely need to be upgraded again since there isn't enough current output to run the vertical motor. This could be avoided if the motor is upgraded instead, but the main driving factor will be the price of the different solutions. For the relay no future updates are needed besides making a housing for the relay and cleaning up the wiring.

9.2 Future Work: Universal Antenna Mount

While the universal antenna mount was successful in increasing the directivity of the measured antennas, there are a couple of aspects of the design that need to be addressed before the completion of this project. Despite attempts to optimize the weight of the antenna mount, the antenna aperture was not able to be held by the current motor system. The current motor controller boards were not providing enough current to the motors so the rated torque for the motors could not be achieved. Future efforts to resolve this issue could include either replacing the antenna aperture mount for a lighter design or replacing the motor controller boards for a higher quality board that is able to supply a sufficient amount of power to the motors so that the maximum amount of torque can be achieved. Addressing this issue would allow future teams to not only conduct cartesian scans but also spherical scans in the antenna testing range.

9.3 Future Work: Near-field to Far-field Transform

There are many things that can be improved with the software to produce better results and increase versatility:

- Make multiple types of field-scans comparably, such spherical and cylindrical. Currently, the only working scan type is rectangular.
- Include multiple components of the scanned EM fields. Currently, only the Y-component of the electric-field was transformed. Which is why it was thought that the radiation patterns as seen in Figure 6.13 is very different from the expected behavior. This only requires adjusting either the probe or transmission antenna's orientation.
- Improve the software's capabilities. Including more detailed plots, implementing a GUI, and error checking improvement.
- Rewrite the software in an open source language that has a more intuitive method for parallelization, such as C++. The surface integral is a very parallelizable problem, but matlab doesn't take as much advantage of that functionality as it could.

REFERENCES

- [1] Ilić, Milan M. "Higher Order Hexahedral Finite Elements for Electromagnetic Modeling." *University of Massachusetts Dartmouth*, IEEE Transactions on Microwave Theory and Techniques, 2003.
- [2] M, Vikass. "IEEE Standard 149-2021: IEEE Recommended Practice for Antenna Measurements" *IEEE Antennas Propag. Mag.*, vol. 64, no. 3, pp 143-143, June 2022, doi: 10.1109/MAP.2022.3162793.
- [3] Valipe, Srivalli. "Antenna Test Facility." NASA, NASA, 24 June 2015, <https://www.nasa.gov/centers/johnson/partnerships/eddc/hsvs/antenna-test-facility>.
- [4] Alsager, Ahmed Fathi. "Design and Analysis of Microstrip Patch Antenna Arrays." *University College of Borås*, 2011.

APPENDICES

Appendix A- Abbreviations

ATR: Antenna Testing Range

CFD: Computational Fluid Dynamics

- Type of analysis conducted on parts to determine flow characteristics around a particular model and provides solutions for fluid dynamics based problems using computers and algorithms.

CNC: Computerized Numerical Control

- Computerized manufacturing process where material (for the purpose of this project, steel) is removed by abrasive cutting tools.

CSU: Colorado State University

ECE: Electrical and Computer Engineering

GUI: Graphical User Interface

HFSS: High-frequency Structural Simulation

MRI: Magnetic resonance imaging

PC: Personal Computer

PLA: Polylactic Acid

- Common type of material used in additive manufacturing processes due to the low cost and the low melting temperatures of the material.

PNA: Precision Network Analyzer

- Synonym for VNA.

QoL: Quality of Life

RF: Radio Frequency

VNA: Vector Network Analyzer

- Synonym for PNA

Appendix B- Budget

Project	Description	Cost
Redundant Storage and Server Integration	N/A	\$0.0
Motor Controller Case	2x Dual Ball Bearing Computer Fan	\$15.57
	1x PLA	Free
	1x Ball Bearing Drawer Slides	\$12.99
	6x Cabinet Door Hinge	\$6.99
	10x Cylindrical Magnet	Free
	1x Computer Case Shell	Free
	1x PSU	\$12.99
	10x Wire Circular Connectors	\$17.03
	Motor Controller Case Cost: \$81.14	
Polar Motor Fix	1x Polar Motor	\$141.99
Motor controller replacement	2x TB6560 4 axis Nema 23 motor controllers	\$110.79
Live Camera Feed of ATR	1x Ethernet Cord	\$5.92
Antenna Aperture Mount	2x 2"x4" 8' Wood Pieces	\$17.50
	1x 24" Steel Shaft	\$16.00
	2x Mounted Bearings	\$60.00
	1x Pine Base	\$12.00
	Screws	\$10.00
	Antenna Aperture Mount Cost: \$115.50	
Near-field to Far-field Transform	N/A	\$0.0
5-Element Patch Antenna Array	7x 50Ω SMA Edge Connector	\$87.19
	3x PCB from Advanced Circuits	\$132.45
	5-Element Patch Antenna Array Cost: \$219.64	
Total Spent: \$674.98 (previously \$416.28 from first semester)		

Appendix C- Project Plan Evolution

Task Class	Task	Task Description	Task Inclusions		Dependencies	Sub-Team Charter
			Yes	TBD		
Quality of Life	• CCTV Camera in ATR	-Allows operator to see how the antenna is moving	- CCTV equipment - Mounted screen for outside of the test range			- Project Lead: Donovan
	• Landline Phone in ATR	-Allows for communications while inside Antenna Test Range				- Project Lead: Donovan
	• Motor Controller Case	- Custom case designed to protect the motor controller hardware.	- Custom case - Case intake/outtake ventilation	- Microcontroller motor controller hardware on/off switch		- Project Lead: Owen
Scan Quality Improvement	• Vertical Poll Stabilization				- Ball Aerospace recommendations	
	• Antenna Mounting Hardware					
	• RF Leakage				- Ball Aerospace recommendations	
Precision	• Ball Aerospace Recommendations					
	→ Hardware Fixes					
	→ Software Fixes					
Antenna Design	• Electronically Steerable Antenna (ESA)				- Dr. Branislav Notaros recommendations	
	• Dipole Antenna				- Dr. Branislav Notaros recommendations	
	• Near & Far Field Translation					- Project Lead: Adam
Data & Equipment	• Scan Data RAID-like Storage Server	- Server that stores scan data.	- Large storage capacity - Software controlled server configuration - Internet connection	- Automatically store scan data	- CSUATRv2 source code	- Project Lead: Josh - Server Hardware: Parker - Server Software: Josh

	• Remote ATR PC	- Remotely run scans using a RDP connection to the ATR PC		- Motor controller case microcontroller on/off switch - Internet connection - CCTV Camera in ATR	- Project Lead: Parker - Microcontroller On/Off: Owen, Donovan
Functionality Evaluation				- Mechanical Eval: Owen, Donovan - Program & Non-Mechanical Eval: Parker, Josh - Scan Eval: Adam	
(Figure 12.1: First Iteration of Task List)					

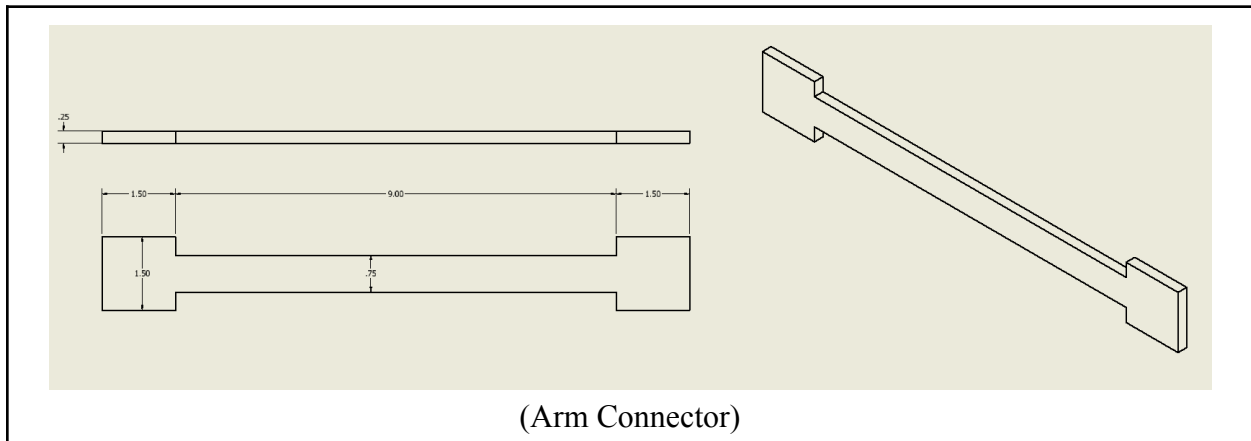
EE	CE	ME
Functionality Evaluation		
Planning (Scan Performance)	Planning (Program & Non-Mechanical)	Planning (Mechanical Components)
Run Scan of Each Axis	Cable Management Check	Rail System Check
Electrostatic Discharge (ESD) Check		Mount For Horn Antenna Evaluation
Test out cylindrical and spherical scan	PNA Surge Protection Check	Evaluate Support Structure for vertical rail system
		Determine Precision and Range of Motors
	Finish	Finish
Scan Data Server		
Planning		
Upgrade ATR PC Hardware		
Install Server Software		
Test and Finish		
QoL Improvements		
		Set up CCTV Camera
		Set up intercom
Equipment Case		
		Create and Finish Design
		Determine Parts Required
		3D Print and Assemble Case
		Create and Code Remote Controlled Microcontroller
		Test and Complete Design
Near-field to Far-field Transform		
Research		
7-Tesla MRI Scan		
	Meet with MRI Team	

(Figure 12.2: First Iteration of Timeline)

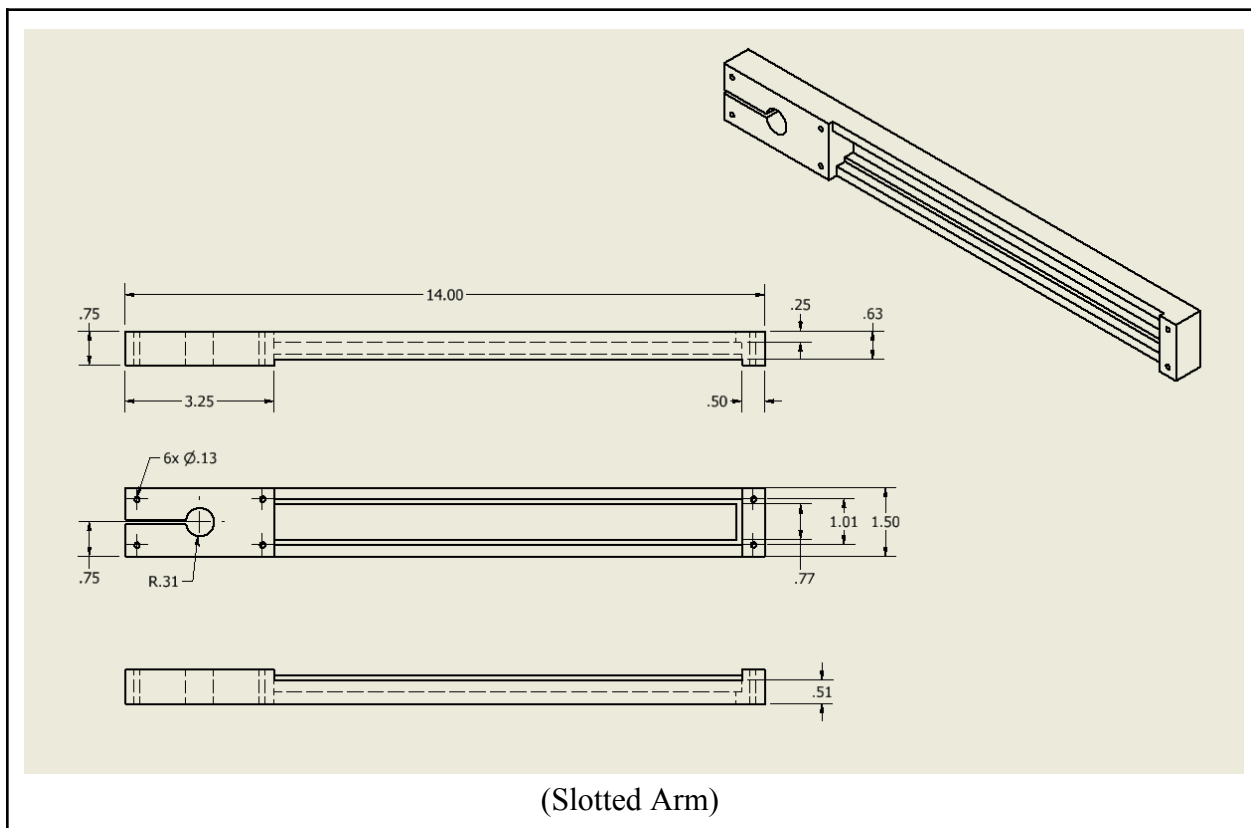
Adam	Parker	Josh	Owen	Donovan
Functionality Evaluation: Scan Performance, Program & Non-Mechanical Components				
Run scan of each axis	Research on PNA Surge/ESD Sensitivity			
Electrostatic Discharge Check	Assess PNA Surge/ESD Vulnerability			
Test Cylindrical and Spherical scan	Implement Additional Protection if Needed			
Develop Report	Review/Create Motor Controller Schematic Reconnect Motor Controller once case is made Perform cable management to prevent hazards Develop Report			
Functionality Evaluation: Mechanical Components				
<u><i>Support Structure Deliverables</i></u>		Determine Customer Requirements Evaluate the Vertical and Horizontal Substructure Develop Report		
<u><i>Transversal Mechanism Deliverables</i></u>		Determine Customer Requirements Evaluate the Pulley System and Axle for Current condition Develop Report		
<u><i>Motor Precision Improvements Deliverables</i></u>		Determine Customer Requirements Evaluate the Current Motor Precision and Range Develop Report		
<u><i>Antenna Mounts Deliverables</i></u>		Determine Customer Requirements Examine Multiple Different Antennas That Need to be Mounted Develop Report Develop Full Report		
Motor Controller Case				
Determine Customer Requirements Design Solution in Solidworks Determine Hardware and Material Needed to Assemble Solution Create Wiring Diagram For Controller Put Device Design into AnsysWorkbench to Determine Airflow In and Out Purchase Commercially Available Parts 3-D Print Solidworks Design Assemble Solution Test and Finalize Design				
NF-FF Transform				
Research		Write Scan Data Parsing Software		
Write NF-FF Transformation Algorithm				
Learn HFSS				
Test NF-FF Transformation Algorithm with HFSS				

			CCTV Live Feed
			Verify Existing Cameras Work Display Live Camera Feed of ATR
			Connect Feed to ATR_PC Create Documentation on how to Setup Camera Feed
			ATR Intercom
			Evaluate ATR for Best Configuration Research Systems on the Market Develop Flowchart based on Available Components Order components Integrate System into Workspace Evaluate + Test reliability Create Documentation On How System Works
		Scan Data Server	
	Connect PC to Internet		
	Install Hard drives into ATR PC		
	Repair ATC PC		
		Install SQL Server Express Connect SQL server with Microsoft Onedrive	
		Change data storage location in Source code	
		Microcontroller Motor Controller On Switch	
	Evaluate Motor Controller Setup		
	Research Components		
	Order Components		
		Review Motor Controller Schematic Integrate System	
		Test and Evaluate	
Rebuild Antenna Center of Rotation			Rebuild Antenna Center of Rotation
Evaluate Current Center of Rotation Mechanism			Evaluate Current Center of Rotation Mechanism
			Design New Center of Rotation Mechanism
Rewire Mechanism			Simulate Model
Scan via New Center of Rotation			Order Components
			Construct Mechanism
			Rewire Mechanism
		Scan the 7-Tesla MRI Coil	
		Meet with MRI Team	
		Scan Coil	
		Develop Coil Scan Report	
			(Figure 12.3: Final Iteration of Timeline)

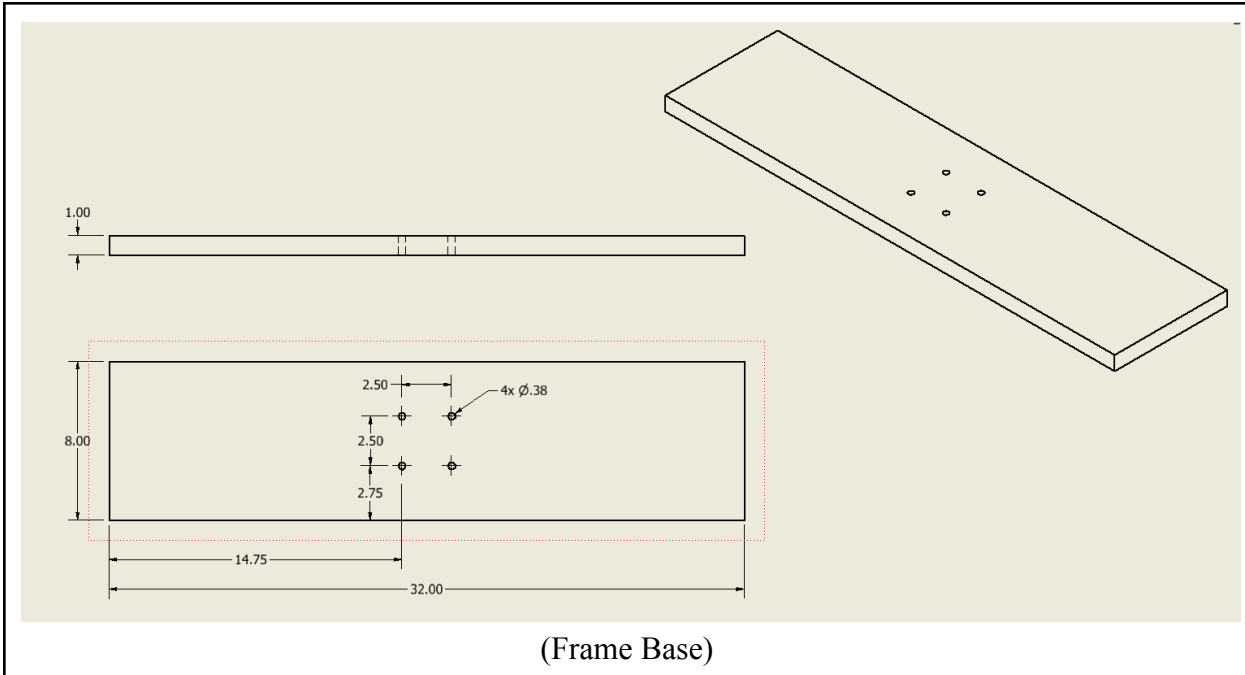
Appendix D: Universal Antenna Mount Drawings



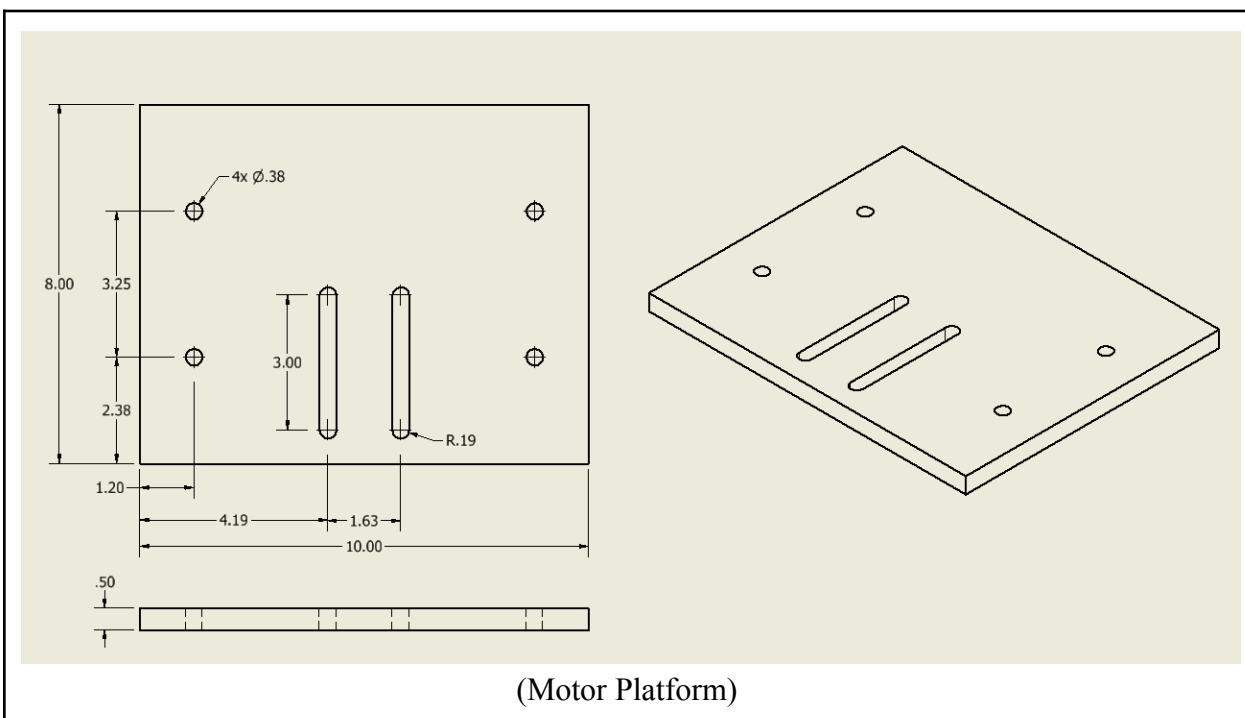
(Arm Connector)



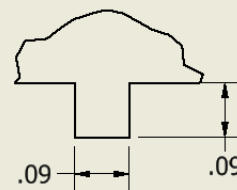
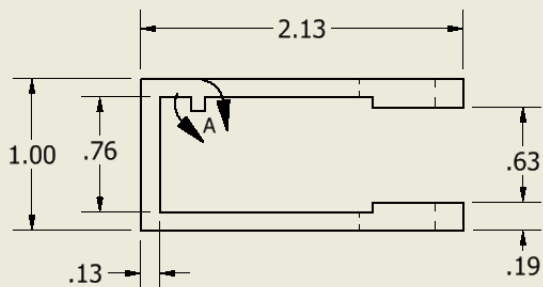
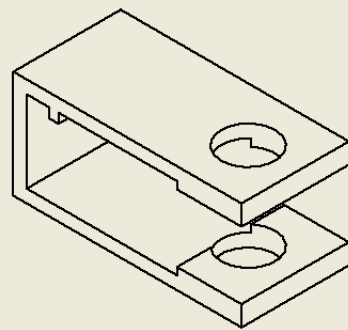
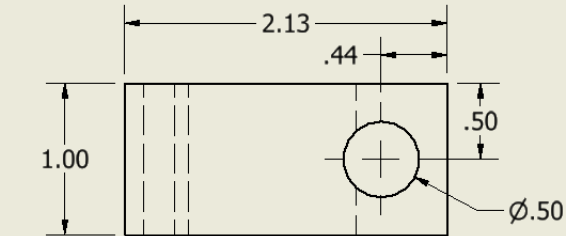
(Slotted Arm)



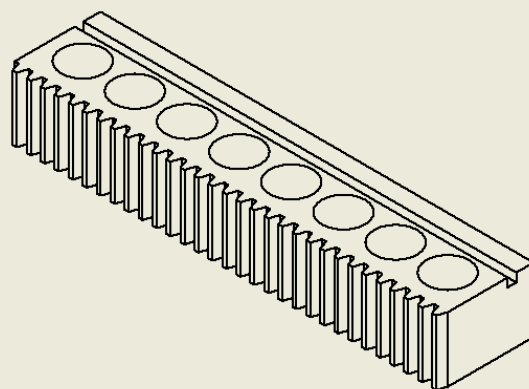
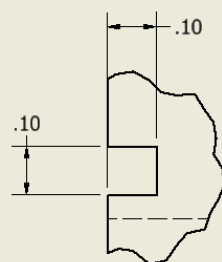
(Frame Base)



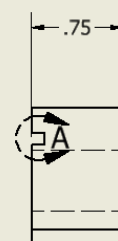
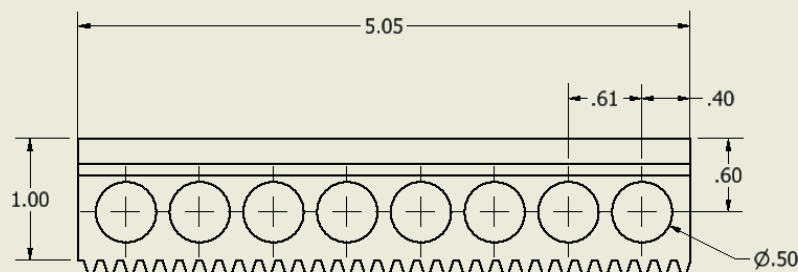
(Motor Platform)



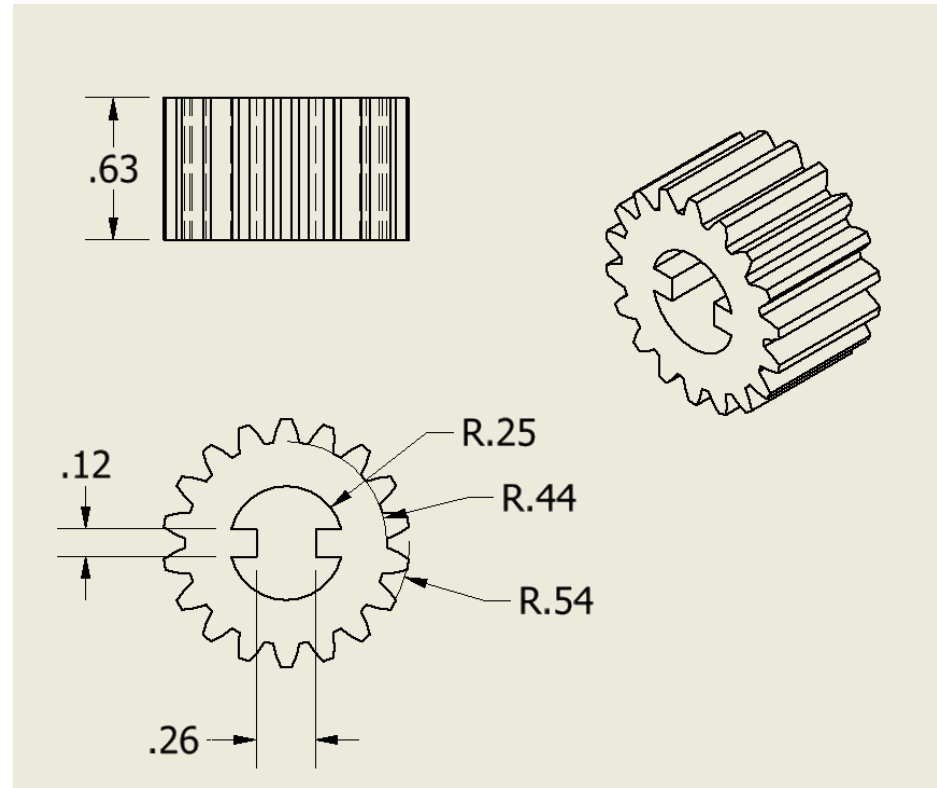
(Collar)



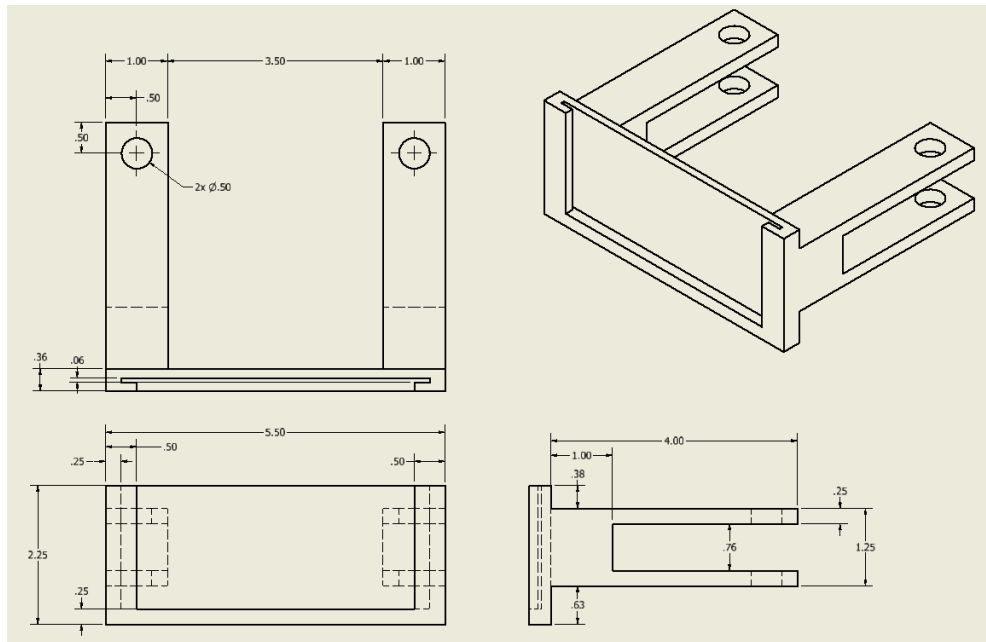
DETAIL A
SCALE 4 : 1



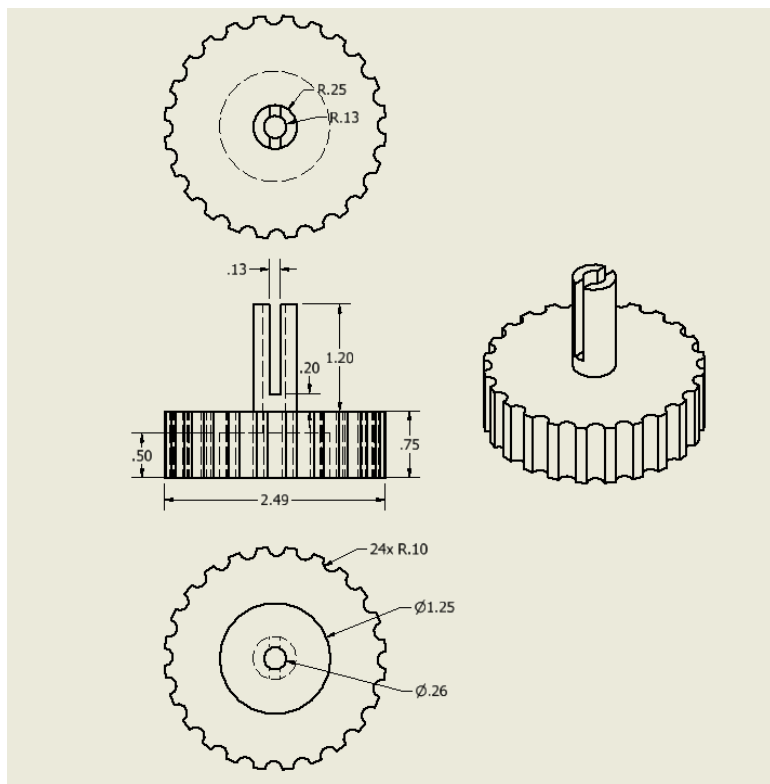
(Collar Rack)



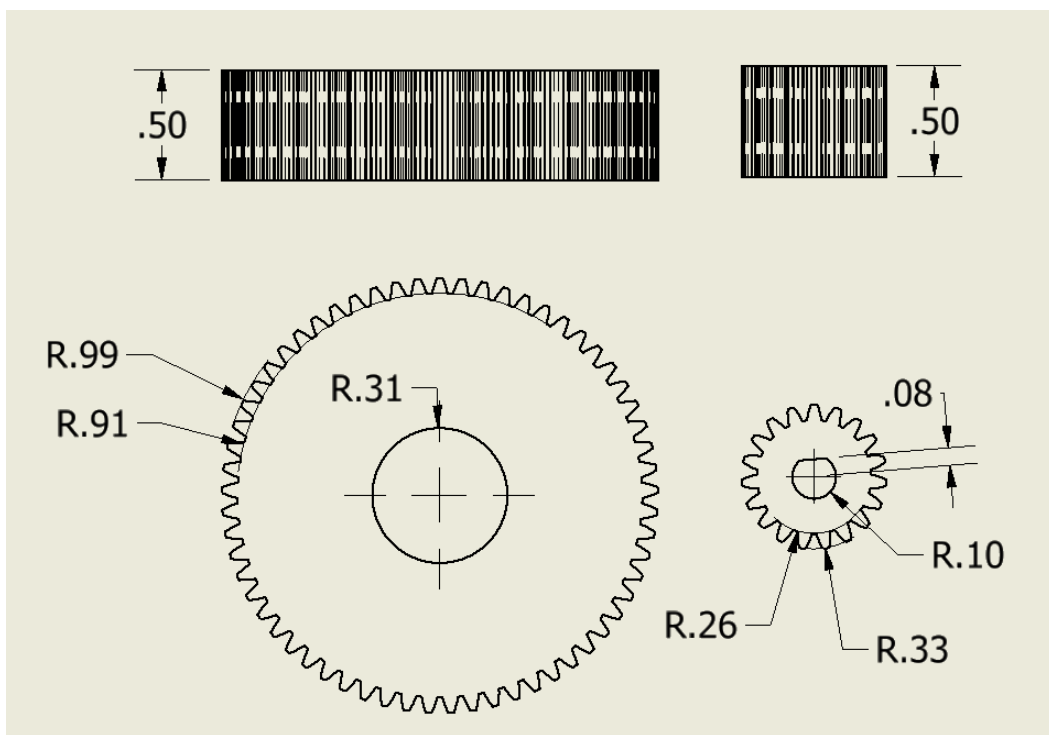
(Collar Pinion)



(Patch Array Mount)



(Knob)



(Motor Gears)

Appendix E: NF->FF Software Operation & Troubleshooting

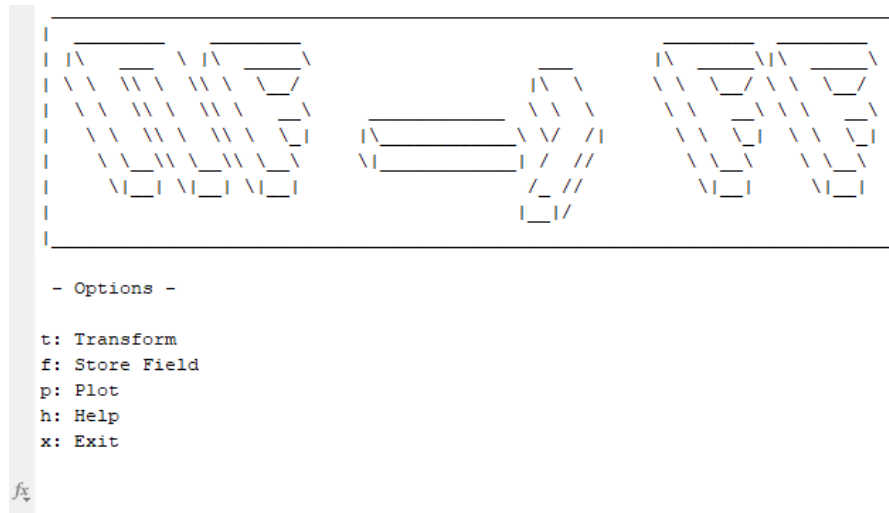
How to Use NF->FF

- ```
Parent File
• Data
 o <.xlsx and .txt files containing EM field data>
• MATLAB
 o Documentation
 ■ About NFtoFF.txt
 ■ NFtoFF Logo.txt
 ■ Program Design.txt
 ■ Providing Data.txt
 ■ Transforming.txt
 o Misc Files
 ■ NFtoFF.psl
 o FunctionContainer.m
 o Interface.m
 o Plotter.m
 o ScanHandler.m
 o SimHandler.m
 o TransformObject.m
 o TransformSweep.m
• NFtoFF.exe
```

(NFtoFF Software Directory Contents)

The following is the procedure on how to use the NF->FF software:

1. Run the NFtoFF.exe from a directory containing files as illustrated in Figure 6.11. It might take a little bit to open, so give it some time.
2. After running the NFtoFF.exe, the following Command Window should appear in MATLAB:



3. Select one of the five options in the menu screen, follow through with the prompts and it should work fine.

The transform object prompts the user for data type, frequency, far-field point, etc. It computes a far-field mesh that can be plotted with the ‘plot’ option. Note that fields are not saved as a file, and only saved in the MATLAB Workspace, which can be accessed from the same MATLAB application page as the MATLAB Command window.

If you wish to store data as a file, you must export the object that contains said data. It will store it as a .mat file, and requires whatever object you saved to be accompanied by the corresponding object file in the same directory if you wish to access it. For example, TransformSweep, SimHandler, and ScanHandler.

### **NF->FF Troubleshooting**

| Problem                              | Potential Fixes                                                                                                                                                                                                                                                                                                                                                                                                                                                                                                                           |
|--------------------------------------|-------------------------------------------------------------------------------------------------------------------------------------------------------------------------------------------------------------------------------------------------------------------------------------------------------------------------------------------------------------------------------------------------------------------------------------------------------------------------------------------------------------------------------------------|
| NF->FF not Opening                   | <ul style="list-style-type: none"> <li>● Make sure all files are in their proper place when running the program as illustrated in Figure 6.11.</li> <li>● Make sure MATLAB is installed on the machine you’re using. All CSU College of Engineering Lab spaces should have MATLAB installed.</li> </ul>                                                                                                                                                                                                                                   |
| Data Not being Interpreted Correctly | <ul style="list-style-type: none"> <li>● Make sure that you are using a rectangular scan. This only works with a rectangular mesh.</li> <li>● If the intended data is simulated, make sure that the data stored in the .xlsx file is correctly formatted. In the NF-&gt;FF menu screen, select ‘help’ and select ‘Providing Data’ for more information.</li> <li>● If the intended data is from an ATR measurements, make sure the .txt file has been unmanipulated. NF-&gt;FF only parses raw text files produced by the PNA.</li> </ul> |
| NF->FF Quits Unexpectedly            | <ul style="list-style-type: none"> <li>● The software wasn’t designed with rigorous error checking in mind. Therefore, if it errors out unexpectedly, it’s likely due to an unexpected input that might have caused it to fail.</li> </ul>                                                                                                                                                                                                                                                                                                |
| General Problem                      | <ul style="list-style-type: none"> <li>● If some unforeseen error occurs, simply follow through with whatever MATLAB produces as an error code.</li> <li>● Debugging with MATLAB is a good option to diagnose unforeseen issues.</li> </ul>                                                                                                                                                                                                                                                                                               |

## **ACKNOWLEDGEMENTS**

We would like to sincerely thank Dr. Branislav Notaros for allowing the CSU ATR team the freedom to explore whatever curiosities interested us both as engineers and students. We would not have had the opportunity to gain so much experience, and to contribute as much as we have and will continue to do for the CSU ATR.

We would like to sincerely thank Dr. Milan Ilić for teaching and providing reference for the Near-field to Far-field Transformation project. Many teams have attempted to develop the transform in the past, but none have succeeded. Dr. Ilić is the only reason this generation of the CSU ATR has come this far with the transform.

We would like to sincerely thank Ball Aerospace for sending down Carlos Arzola and Mike Dolan, to take a look at the CSU ATR and give their own personal recommendations on various improvements that could be made. It was extremely helpful and insightful to the team as a whole to hear how their own ATR operates and get feedback in regards to each discipline.